Interactive comment on "The impact of Pacific Decadal Oscillation on springtime dust activity in Syria" by Bing Pu and Paul Ginoux
Anonymous Referee #2
Received and published: 7 September 2016

We thank the reviewer for very helpful comments. Our replies to the comments (in Italic) are listed below.

This study examined the influences of the Pacific decadal oscillation (PDO) on dust activities in Syria using an innovative dust optical depth (DOD) dataset derived from Moderate Resolution Imaging Spectroradiometer (MODIS) Deep Blue aerosol products. In this paper the authors used both model and observations and it will be good if they can talk to how they both complement each other. What are the reasons for the discrepancies? Are there any sensitivity tests?

We added lines 227-229, 537-539 to better discuss how model results may complement satellite observations in the recent decade by providing a longer time series (i.e., 51 years) to examine the connection between the PDO and Syrian DOD. The discussion on the discrepancies between model results and observations are also better organized in lines 539-553. Current GFDL model can only partially reproduce the negative connection between Syrian DOD and the PDO in spring due to the limitation of the dust emission scheme, the influence of soil moisture on dust emission will be included in our newer version of the model, and we plan to conduct sensitivity tests to further quantify the influence of the PDO on Syrain DOD in the future.

Since the authors are attempting to study the impact of PDO on dust activities using mainly satellite data and PDO is tied to ENSO as mentioned by the authors, wont you think you have selected a quite short time period that is not good enough to establish the link raised by the authors? Why dust models are not used in this analysis to cover much longer time periods? Ex (Skiron, Dream and others?

The reviewer questioned why a quite short time period is selected to examine the relationship between Syrian DOD and the PDO.

2003-2015 is selected due to the time coverage of MODIS Deep Blue aerosol products. We demonstrated in the paper that the PDO index and Syrian DOD are not only statistically significantly correlated in the recent 13 years (section 3) but also physically connected with each other (section 4). We totally agree that due to the multi-decadal variability of the PDO (15-25 and 50-70 years) the results will be more robust if longer time series of the observations are available. In the paper, we tried to use a method to indirectly verify the relationship between the two during 1948-2015 (the second paragraph in section 4 in the old version). We have modified lines 301-316 to better discuss this method. First, we identify the key meteorological conditions associated with

Syrian DOD in the recent decade. Then we compare the influences of the PDO on meteorological conditions during 2003-2015 to a longer period (e.g., 1948-2015). If the PDO shows a relatively consistent influence on the meteorological conditions that are critical to Syrian DOD activities, and assuming that the connection between the DOD activities and those meteorological conditions does not change much during 1948-2015, then the influences of the PDO on Syrian DOD are also likely to persist in this time period.

We added lines 549-553 to explain why we did not use dust model as the major tool to examine the connection of the PDO and Syrian DOD. Global climate model would be a great tool to study long-term variations of DOD and factors influence DOD variability if the model can sufficiently reproduce the variability of DOD. However, current dust models still have difficulties to fully capture the dust surface concentration and those vertically integrated variables such as aerosol optical depth, with a inter-modal differences of a factor of two (Huneeus et al. 2011). Results from CMIP5 model simulations also suggest that current global models barely capture the interannual to decadal variations of the dust activities (e.g., Evan et al. 2014). The GFDL CM3 model discussed in section 6 also shows a weaker connection between the PDO and Syrian DOD compared to the observation due to model's limitation to reproduce the variability of the DOD.

The regional dust forecast models mentioned by the reviewer are very useful tools for short-term forecasts, however, how and whether these models can reproduce interannual or decadal variability of dust in Syria are not clear. On the other hand, regional dust models usually require meteorological fields as initial and lateral boundary conditions to drive the model. Therefore, the temporal coverage of this kind of analysis will also be limited by the coverage of reanalysis products that used to drive the model, which are usually shorter than 100 years and thus cover only one multi-decadal cycle of the PDO.

References:

Evan, A. T., Flamant, C., Fiedler, S., and Doherty, O.: An analysis of aeolian dust in climate models, Geophys. Res. Lett., 41, 5996–6001, doi:10.1002/2014GL060545, 2014.

Huneeus, N, Schulz, M., Balkanski, Y., and et al.: Global dust model intercomparison in AeroCom phase I, Atmos. Chem. Phys., 11, 7781–7816, 2011.

The impact of Pacific Decadal Oscillation on springtime dust activity in Syria

Bing Pu[1,2] and Paul Ginoux[1,2]

[1]Atmospheric and Oceanic Sciences Program, Princeton University,

Princeton, New Jersey 08544

[2]NOAA Geophysical Fluid Dynamics Laboratory, Princeton, New Jersey 08540

Correspondence to: Bing Pu, Bing.Pu@noaa.gov

Abstract. The increasing trend of aerosol optical depth in the Middle East and a recent severe dust storm in Syria have raised questions as whether dust storms will increase and promoted investigations on the dust activities driven by the natural climate variability underlying the ongoing human perturbations such as the Syrian civil war. This study examined the influences of the Pacific decadal oscillation (PDO) on dust activities in Syria using an innovative dust optical depth (DOD) dataset derived from Moderate Resolution Imaging Spectroradiometer (MODIS) Deep Blue aerosol products. A significantly negative correlation is found between the Syrian DOD and the PDO in spring from 2003-2015. High DOD in spring is associated with lower geopotential height over the Middle East, Europe, and North Africa, accompanied by near surface anomalous westerly winds over the Mediterranean basin and southerly winds over the eastern Arabian Peninsula. These large-scale patterns promote the formation of the cyclones over the Middle East to trigger dust storms and also facilitate the transport of dust from North Africa, Iraq, and Saudi Arabian to Syria, where the transported dust dominates the seasonal mean DOD in spring. A negative PDO not only creates circulation anomalies favorable to high DOD in Syria but also suppresses precipitation in dust source regions over the eastern and southern Arabian Peninsula and northeastern Africa.

On the daily scale, in addition to the favorable large-scale condition associated with a negative PDO, enhanced atmospheric instability in Syria associated with increased precipitation in Turkey and northern Syria is also critical for the development of strong springtime dust storms in Syria.

1. Introduction

Dust aerosol is an important component in the climate system that can modify global and regional energy and water balances (e.g., Tegen et al., 1996; Miller and Tegen, 1998; Miller et al., 2004; Lau et al., 2009; Yue et al., 2010; 2011; Choobari et al., 2014; Huang et al., 2014). Dust particles interact with both solar and terrestrial radiation, modifying temperature profile and hydrological cycle, which impact regional and global climate. For instance, studies found that mineral dust influences the strength of the West African monsoon (e.g., Miller and Tegen, 1998; Miller et al., 2004; Yoshioka et al., 2007; Solmon et al., 2008; 2012; Mohowald et al., 2010; Strong et al., 2015) and Indian summer monsoonal rainfall (Vinoj et al., 2014; Jin et al., 2014, 2015, 2016; Solmon et al., 2015; Kim et al., 2016). Dust particles can also serve as ice cloud nuclei and influence the microphysical and macrophysical properties of the cloud (e.g., Levin et al., 1996; Rosenfeld et al., 1997; Wurzler et al., 2000; Nakajima et al., 2001; Bangert et al., 2012), including its droplet size, number concentration, lifetime, albedo, and in turn affecting the regional radiative budget and hydrological cycle. Mineral dust also provides nutrients for ocean phytoplankton, affecting ocean productivity and therefore carbon and nitrogen cycles and ocean albedo (e.g., Fung et al., 2000; Shao et al., 2011). Strong dust storms also have severe social and health impacts (e.g., Morman and Plumlee, 2013), affecting public transportation and causing damage to the eye and lung.

The Middle East is one of the dustiest regions in the world, and recent study suggested an increasing trend of aerosol optical depth largely due to dust emission (e.g., Pozzer et al., 2015; Klingmüller et al., 2016). A once-in-ten-years severe dust storm recently occurred in Syria during September 6-9th, 2015, and raised many attentions. More than one thousand people in

Syria were hospitalized due to breathing difficulties*. The causes of such a strong dust storm are not fully understood, but there have been speculations that the ongoing civil war in Syria is largely responsible for it. The argument is that crop fields were abandoned or destroyed by the war, so soil dust is easier to be uplifted by wind from these unprotected land fields. More importantly, will severe dust storms like the one above increase in the future?

Notaro et al. (2015) studied the dust activities over the Arabian Peninsula and related the increased dust activities during 2007-2013 to the persistent dry condition over the "Fertile Crescent" (namely Syria, Iraq, Israel, and Jordan) primarily caused by a combined effect of La Niña and a negative phase of Pacific decadal oscillation (PDO). Associated with the drought is crop failure and increased dust activities over the Arabian Peninsula. While others, such as Chin et al. (2014) found that the positive trend of dust emission over the Middle East from 2000-2009 is related to increased surface wind speed, and Klingmüller et al. (2016) attributed the positive trend of aerosol optical depth (AOD) over the region (mainly Saudi Arabia, Iraq, and Iran) from 2001-2012 to a combined effects of decreased precipitation and soil moisture over Iraq and adjacent areas and enhanced surface wind over the Africa Red Sea coastal area that increased dust emission.

The above studies suggested that remote sea surface temperature (SST), local precipitation, surface wind, and vegetation all influence the dust activities over the Middle East. Among these factors, the remote forcings, such as tropical Pacific SST, the PDO, not only affect the precipitation variations over the region but can also influence local circulation including near surface winds, both of which influence dust emission. It is thus quite important to understand the

* https://www.washingtonpost.com/news/worldviews/wp/2015/10/07/syrias-war-helped-create-an-epic-dust-storm-scientists-say/

91 influences of these low-frequency long-lasting forcings on dust activities underlying the ongoing
92 human perturbations such as civil war, land use change, and anthropogenic emission.
93 In this paper we examine the influence of the PDO on the variations of dust activities in
94 Syria from 2003-2015 using Moderate Resolution Imaging Spectroradiometer (MODIS) Deep
95 Blue dust optical depth (DOD). Previous studies on the connection between the PDO and dust
96 activities in the Arabian Peninsula mainly focus on precipitation (e.g., Notaro et al., 2015; Yu et
97 al., 2015). Here we explore thoroughly how the PDO influences the key factors associated with
98 the dust activities in Syria on the interannual and daily scales.
99 The following section presents the data and methodology used in the paper. The co-
100 variations of DOD in Syria and PDO from 2003-2015 are presented in sections 3 and their
101 physical connections are analyzed in details in section 4. We also discussed the long-time
102 connection (e.g., 1948-2015) between Syrian DOD and the PDO inferred from the reanalyses
103 and observations in section 4. In section 5, we examined the key factors associated with strong
104 spring dust events in Syria using daily reanalysis and observations. To what extend can climate
105 models capture the connections between the PDO and Syrian dust activities is ~~examined~~
106 discussed using the Geophysical Fluid Dynamics Laboratory (GFDL) AM3 model ~~and discussed~~
107 in section 6. Major conclusions are summarized in section 7.
108
109 **2. Data and methodology**
110 **2.1 Satellite and observational datasets**
111 **2.1.1 Dust optical depth**
112 Daily and monthly dust optical depth data is derived from MODIS aerosol products
113 retrieved using Deep Blue (M-DB2) algorithm, which employs radiance from the blue channels

to detect aerosols over bright land surface (e.g., desert). Because surface reflectance is low at blue channels, increases of reflectance and spectral contrast indicate the presence of aerosols (Hsu et al., 2004, 2006). Ginoux et al. (2012) used collection 5.1 level 2 aerosol products from MODIS aboard Aqua satellite to derive DOD. Here, both MODIS aerosol products (collection 6, level 2) from the Aqua and Terra platforms are used for cross-validation. Terra passes the equator from north to south around 10:30 a.m. local time while Aqua passes the equator from south to north around 13:30 p.m. local time. While the frequency of the maximum daily 10 m wind in Syria peaks in the afternoon, later than the passing time of both Terra and Aqua, the averaged maximum total wind speed is nearly evenly distributed over a day (supplementary Figure S1). Thus, the results from both platforms are likely to provide a more complete picture of dust activities than either one alone.

Aerosol products such as AOD, single scattering albedo, Angström exponent are first interpolated to a regular 0.1° by 0.1° grid using the algorithm described by Ginoux et al. (2010). The dust optical depth is then derived from AOD following the methods of Ginoux et al. (2012) with adaptions for the newly released MODIS Collection 6 aerosol products. To separate dust from other aerosols, we use the Angström exponent, which has been shown to be highly sensitive to particle size (Eck et al., 1999) and single scattering albedo which is less than one for dust due to its absorption of solar radiation. Instead of using negative values of Angström exponent as by Ginoux et al. (2012), we use a continuous function relating Angström exponent to fine-mode aerosol optical depth established by Anderson et al. (2005; their Eq. 5) based on ground-based data. The DOD data is available from January 2003 to December 2015.

Daily and monthly DOD indices are formed by averaging DOD data in Syria between 34°-36.5°N and 36.5°-41°E to characterize dust activities. The averaging area covers most region

of Syria. We also tested using a smaller averaging box (33.5° -36°N, 36.5°-39°E) for the DOD index, and the results are similar.

2.1.2 Precipitation

Version 7 of Tropical Rainfall Measurement Mission (TRMM) Multi-satellite Precipitation Analysis (TMPA) daily product (3B42) is used. This product covers from 50°S to 50°N with a spatial resolution of 0.25° by 0.25° and is available from 1998 to present. Several important changes are applied to version 7 product, including using additional satellite data such as early record of Microwave Humidity Sounder (MHS) and operational Special Sensor Microwave Imager (SSM/I) record, using a new infrared brightness temperature dataset before the start of the Climate Prediction Center (CPC) 4-km Merged Global IR data set, using a single uniformly processed surface precipitation gauge analysis, using a latitude-band calibration scheme for all satellites, and adding output fields in the data files (Huffman and Bolvin, 2014).

Precipitation Reconstruction over Land (Chen et al., 2002; hereafter PRECL) from National Oceanic and Atmospheric Admiration (NOAA) is a global analysis available monthly from 1948 to present at a 1° by 1° resolution. The dataset is derived from gauge observations from the Global Historical Climatology Network (GHCN), version 2, and the Climate Anomaly Monitoring System (CAMS) datasets.

The monthly precipitation of the Climatic Research Unit (CRU) time-series (TS) 3.23 (Harris et al. 2014) is also used as a supplement to the PRECL. CRU TS 3.23 dataset covers 1901-2014, with a spatial resolution of 0.5° by 0.5° over land (excluding Antarctica). The gridded data is based on the analysis of over 4,000 individual weather station records.

2.1.3 Temperature

160 The Hadley Centre sea ice and sea surface temperature (HadISST) data set (Rayner et al.,
161 2003) from the UK Met Office is available monthly from 1870 to the present with a horizontal
162 resolution of 1° by 1° grid. Monthly SST from HadISST and land surface temperature from CRU
163 TS 3.23 (0.5° by 0.5°) from 1948-2015 are used to examine temperature patterns associated with
164 dust activities.
165
166 **2.1.4 Leaf area index (LAI)**
167 LAI characterizes the canopies of plants. It is defined as the one-sided green leaf area per
168 unit ground area in broadleaf canopies and as half the total needle surface area per unit ground
169 area in coniferous canopies. LAI at zero is considered as bare ground while around 10, dense
170 forests. Monthly LAI is derived from the version 4 of Climate Data Record (CDR) of Advanced
171 Very High Resolution Radiometer (AVHRR) surface reflectance (Claverie et al., 2014) and
172 produced by the National Aeronautics and Space Administration (NASA) Goddard Space Flight
173 Center (GSFC) and the University of Maryland. The gridded monthly data is on a 0.05° by 0.05°
174 horizontal resolution and available from 1981 to present. A detailed discussion on the algorithm
175 and evaluation of the dataset can be found by Calverie et al. (2016).
176 Monthly MODIS LAI level 4 data on the Aqua platform (MYD15A2) is also used for
177 2003-2015. The original data files were obtained via personal communication (Ranga Myneni
178 and Taejin Park; Boston University) and then reprocessed to fill the missing data by Paul
179 Ginoux. The horizontal resolution of the data is 0.1° by 0.1° degrees.
180
181 **2.2 Reanalyses**

Daily and monthly geopotential height, horizontal winds, specific humidity from the National Centers for Environmental Prediction (NCEP)/National Center for Atmospheric Research (NCAR) reanalysis (Kalnay et al., 1996, hereafter NCEP1) from 1948 to 2015 are used. Its horizontal resolution is 2.5° by 2.5° and have 17 vertical levels from 1000 hPa to 10 hPa, with 8 levels between 1000 hPa and 300 hPa. This reanalysis is used primarily in this study due to its long record.

ERA-interim (Dee et al., 2011) from the European Centre for Medium-Range Weather Forecasts (ECMWF) is a global reanalysis with a horizontal resolution of T255 (about 0.7° or 80 km) and 37 vertical levels, available from 1979 to present. Monthly and four (two) times daily analysis (forecast) variables are used. The time coverage of ERA-Interim is shorter than the NCEP1 but its high resolutions supplements the latter. Monthly horizontal winds and geopotential heights are compared with the NCEP1 in the same period (1979-2015) and show similar features (see discussion in section 3). Daily 10 meter and 850 hPa winds, and forecast variables such as precipitation are used to investigate the key factors associated with dust activities.

2.3 Climate indices

The PDO and Niño3.4 indices are downloaded from the website of NOAA Climate Prediction Center (http://www.esrl.noaa.gov/psd/data/climateindices/list/). The monthly standardized PDO index is derived from the leading principal component of SST anomalies in the northern Pacific Ocean (20°N north). The monthly mean of global mean SST anomalies are removed in the PDO index, thus the influence of global warming is not included. The data is available from 1948 to present. The monthly Niño 3.4 index is derived from the extended

reconstructed sea surface temperature (ERSST v4; Huang et al., 2015; Lui et al., 2015; Huang et al., 2016) averaged over the tropical Pacific between 5°N–5°S and 120°–170°W and is available from 1950 to present.

2.4 Model output

To examine the relationship between the Syrian dust activities and the PDO, the output from the atmospheric component (AM3) of a general circulation model (CM3; Donner et al., 2011) developed at the GFDL is used. The finite-volume algorithms described in Lin and Rood (1996, 1997) and Lin (1997, 2004) is used in the dynamic core in AM3. Different from earlier versions of the model, a general curvilinear coordinate system is used and largely improved the computational efficiency. A hybrid vertical coordinate (Simmons and Burridge, 1981) of 48 layers is used, with the top model layer at about 1 Pa (~86 km). AM3 calculates the mass distribution and optical properties of aerosols according to their emission, chemical production, transport, and dry and wet deposition. The dust source function follows the scheme of Ginoux et al. (2001), which places preferential sources in topographic depressions. The simulated aerosol optical depth and co-albedo show improved correlations with the AErosol RObotic NETwork (AERONET) station observations than earlier version of the model (CM2.1) but slightly underestimate AOD in the Middle East.

A historical run is conducted using the observed monthly SSTs from the Hadley center to drive the AM3. The simulated wind is nudged toward the NCEP/NCAR reanalysis with a relaxation timescale of 6 hours (Moorthi and Suarez, 1992), similar to the method used by Li et al. (2008). A moderate horizontal resolution of 2° by 2.5° is used. The simulation was conducted from 1948 to 2010. Results from 1960 to 2010 are presented. The simulation provides slightly

longer time series compared to the satellite data to examine the relationship between Syrian DOD activities and the PDO.

3. The co-variations between springtime DOD in Syria and the PDO during 2003-2015

Notaro et al. (2015) related low-frequency variations of monthly precipitation over Syria and Iraq to the El Niño–Southern Oscillation (ENSO) and the PDO and thus built the connection between dust activities and Pacific SSTs. Here we focus on Syria. Figure 1 shows the time series of monthly Syrian DOD indices (seasonal cycle removed) from both MODIS Aqua (green) and Terra (grey) platforms and the negative PDO index from January 2003 to December 2015. The variations of the DOD and the negative PDO indices are quite similar, showing strong decadal variations underlying interannual variations. Both are relatively weak during 2003-2007, relatively strong during 2007-2012 and become relatively weak since 2013. Note that the DOD indices increase again in 2015 in association with the severe dust storm in September. The correlation between monthly DOD indices and PDO index are -0.51 (Aqua) and -0.50 (Terra) from 2003-2015. Other indices, such as Niño 3.4 and Syrian LAI also have significant but lower correlations with the DOD indices (Table 1).

ENSO is known to influence precipitation over the Middle East, by decreasing precipitation in La Niña years and increasing precipitation in El Niño years (e.g., Price et al., 1998; Mariotti et al., 2005; 2007, Chakaborty et al., 2005; Barlow et al., 2002, Wang et al., 2014; Yu et al., 2015; Banerjee and Kumar, 2016), and its influence is generally stronger in La Niña years (e.g., Wang et al., 2014). Previous study also showed a comparable influence of the PDO on precipitation over the "Fertile Crescent" region including Syria and Iraq versus that by ENSO (correlations of 0.52 versus -0.57 from 1979-2013, Notaro et al., 2015). The correlations in this

study indicate that the PDO plays a greater role than ENSO in modulating dust activities in Syria in the recent decade. The PDO is not completely independent of ENSO, but can be viewed as a phenomenon driven by multiple physical processes, including the tropical Pacific SST, atmospheric noise, Aleutian low, Kuroshio-Oyashio Extension, Pacific-North American pattern, Rossby wave breaking and etc. (e.g., Evans et al., 2001; Newman et al., 2003; Schneider and Cornuelle, 2005; Strong and Magnusdottir, 2009; Mills and Walsh, 2013). While some modeling studies suggested that up to half of the variance of the PDO can be explained by ENSO (e.g., Alexander et al., 2002; Liu and Alexander, 2007), others found that there certain part of extra-tropical Pacific SST variability are totally independent of ENSO (e.g., Zhang et al., 1997; Deser and Blackmon, 1995; Zhang and Delworth, 2015). Here the correlation between the monthly PDO and Niño 3.4 indices is 0.63 from January 2003 to December 2015, suggesting that statistically the Niño 3.4 index explains about 40% of the variances of the PDO index.

Figure 2 shows the correlation between the PDO index and Aqua and Terra DODs in spring, along with correlations between the Syrian DOD indices and PDO index in individual month and on annual mean from 2003-2015. The correlation pattern between the PDO index and Aqua DOD is very similar to that associated with Terra DOD (Figs. 2a-b), with negative correlations over most areas of Syria and a stronger correlation over the eastern Syria than the western part. DOD over Iraq and northern Saudi Arabia is also significantly negatively correlated with the PDO. The correlation between the monthly PDO and Syrian DOD indices shows a persistent negative relationship through the year, with higher correlations during March-April-May and also in July-August and December (Fig. 2c). The low correlation in September is due to the severe dust storm in 2015. The seasonal mean correlations between the DOD indices and the

PDO index in MAM are -0.90 for both the Aqua DOD and Terra DOD indices, again much higher than their correlations with other indices (Table 2).

The connection between the Syrian DOD and PDO is further examined in Figure 3, which shows the correlations between the Syrian DOD indices and SST and land surface temperatures during MAM and on the annual mean, along with SST and land surface temperature patterns associated with the PDO index. As shown in Figs. 3a-b, the SST pattern associated with the positive phase of the PDO in spring are quite similar to that in the annual mean, with anomalous warm SST over the tropical Pacific and along the east basin of North Pacific and anomalous cold SST over the subtropical central to western North Pacific. SST in the India Ocean is also positively associated with the PDO. But the correlation between land surface temperature and the PDO is not significant in most regions, including the Arabian Peninsula.

Correlations between Aqua DOD index and SST in MAM are nearly opposite to those of the PDO, with negative correlations over the tropical and eastern Pacific but positive correlations over the central North Pacific (Fig. 3c). Correlations between the annual mean Aqua DOD index and SST and land surface temperature are similar to that in spring, but with slightly weaker magnitude over the central Pacific (Fig. 3d). The temperature patterns correlated with the Terra DOD index are quite similar to that of Aqua DOD index (Figs. 3e-f). Both DOD indices are not significantly correlated with the land surface temperature over the Middle East in spring.

Since Figs. 2-3 indicate a stronger negative correlation between the PDO and Syrian DOD index during MAM than on annual mean or other seasons, the following analysis focuses on their connections in spring. Spring is also the time when Syrian DOD is high and dust storms are most active (supplementary Figures S2-3).

296 **4. How does the PDO affect Syrian dust activities in spring?**

297 In this section we explore the mechanisms underlying the strong negative correlations
298 between the PDO and Syrian DOD indices. Since MODIS DOD only covers the recent decade
299 and the PDO has low-frequency decadal variations with cycles of about 15-25 and 50-70 years
300 (e.g., Minobe, 1997; Mantua and Hare, 2002), it is difficult to assess their long-term (i.e., beyond
301 the recent decade) relationship directly. We tried a method to indirectly verify their connections
302 during 1948-2015 using high quality reanalyses and observation. The PDO shows a dominant
303 negative phase during the late 1940s to 1970s and turns into a dominant positive phase during the
304 1980s and 1990s and becomes mostly negative again since the middle 2000s (e.g.,
305 JISAO/University of Washington website[†]). Therefore the NCEP1 reanalysis covers about one
306 50-70 years multi-decadal cycle of the PDO, while the EAR-Interim covers about half of the
307 cycle.

308 ~~To establish their connections,~~ W~~w~~e first compare the patterns of circulation and
309 precipitation associated with DOD and PDO indices during 2003-2015 to identify key
310 meteorological conditions associated with Syrian DOD activities and how these conditions are
311 connected with the PDO. Then we compare the influences of the PDO on meteorological
312 conditions during 2003-2015 to a longer period (e.g., 1948-2015). If the PDO shows relatively
313 consistent influences on the meteorological conditions that are critical to Syrian DOD activities,
314 then the influences of the PDO on Syrian DOD are also likely to persist during 1948-2015,
315 assuming that the connection between Syrian DOD activities and those meteorological
316 conditions does not change much during 1948-2015.~~The patterns associated with long-term~~
317 ~~variations of the PDO (e.g., 1948-2015 from the NCEP1 or 1979-2015 from the ERA-interim)~~
318 ~~are then examined and compared with those associated with the PDO in the recent decade~~. ~~The~~

[†] http://research.jisao.washington.edu/pdo/graphics.html

~~PDO shows a dominant negative phase during the late 1940s to 1970s and turns into a dominant positive phase during the 1980s and 1990s and becomes mostly negative again since the middle 2000s (e.g., JISAO/University of Washington website‡). Therefore the NCEP1 reanalysis covers about one 50-70 years multi-decadal cycle of the PDO, while the EAR-Interim covers about half of the cycle. Assuming that the factors dominated the variations of Syrian DOD persist beyond the recent decade (e.g., also valid during 1948-2015), then the similarity between the patterns associated with the PDO in the recent decade and those over longer time periods would indicate a persistent influence of the PDO on dust activities in Syria.~~

How does the PDO affect the circulation over the Middle East? Figure 4 shows the regression of 200 hPa (contours) and 850 hPa (shading) geopotential heights onto the standardized PDO and DOD indices. Fig. 4a shows in the positive phase of PDO, stationary wave propagates from the North Pacific through North America, northern Atlantic and Europe to the Middle East. The regressions at 850 hPa are generally similar to those at 200 hPa, indicating an equivalent barotropic structure. Anomalous positive geopotential height over the Arabian Peninsula is associated with a positive PDO during 2003-2015 (Fig. 4a) and also during 1948-2015 (Fig. 4c). The geopotential height patterns associated with the both Aqua and Terra DOD indices are nearly opposite to those associated with the positive PDO index, with anomalous high over the central North Pacific and northeastern North America and anomalous low over the west coast of North America and Europe and the Middle East (Figs. 4b, d).

Fig. 4 suggests that the PDO can influence the variations of springtime DOD in Syria through its modification on the circulation over the Middle East. A negative PDO reduces the geopotential height both at 850 and 200 hPa over the Arabian Peninsula, a scenario that favors high DOD in spring.

~~‡ http://research.jisao.washington.edu/pdo/graphics.html~~

342 The connection between Syrian DOD and 850 hPa winds and geopotential heights are
343 further examined in Figure 5. Fig. 5a shows that a positive PDO is associated with anomalous
344 easterly winds north of 40°N, anomalous northerly winds over the central Mediterranean Sea
345 around 15°E and weak southeasterly winds over the eastern Mediterranean Sea and western
346 Syria in the recent decade (Fig. 5a) and from 1948-2015 (Fig. 5c). Anticyclonic winds are
347 located over Oman and Yemen at the south coast of Arabian Peninsula accompanied by an
348 anomalous high. Positive geopotential height anomalies are also located over the northwestern
349 Africa, and East Africa. On the other hand, winds associated with high Syrian DOD indices are
350 anomalous westerly over the northern Mediterranean basin and Syria (Figs. 5b and d).
351 Anomalous cyclonic flows are located over the southern Arabian Peninsula, nearly opposite to
352 that associated with the positive phase of the PDO. The overall lower geopotential height over
353 the Middle East and Africa also facilitate the formation of the cyclones (such as Sharav
354 cyclones) that are important for the spring peak of dust storms in the northern Arabian Peninsula
355 (e.g., Shao et al. 2001; Israelevich, et al. 2003; Dayan et al. 2008; Dayan et al. 2012).
356 The regression patterns of 850 hPa winds and geopotential height onto the PDO and
357 DOD indices in the ERA-Interim are generally consistent with those shown in the NCEP1
358 (Supplementary Figure S4).
359 Next we examine the associated variations of near surface wind and precipitation that are
360 tied to these geopotential height and low-level wind patterns. Figure 6 shows the regression of
361 10 m winds (vectors) and the cubic 10 m wind speed (shading) in the ERA-Interim onto
362 standardized PDO index and onto the Aqua and Terra DOD indices. The ERA-Interim is chosen
363 here because of its higher horizontal resolution compared to the NCEP1, and thus is more
364 suitable to examine surface wind variations associated with dust blasting in small scales. Cubic

wind speed is used here as classical dust emission scheme relates dust flux to the third power of 10 m horizontal winds. The patterns of the surface wind associated with the DOD indices (Figs. 6b and d) are largely similar to that of winds at 850 hPa (Figs. 5 and S4). Anomalous southwesterly winds from coastal North Africa and over the Mediterranean Sea tend to bring dust from North Africa to Syria. Such a route of dust transport has not been directly examined, but was discussed in back trajectories studies on the airflow patterns onto Israel (e.g., Dayan, 1986). Earlier studies also have suggested a transport of dust from North Africa to the Mediterranean basin (e.g., D'Almeida, 1986; Moulin et al., 1998; Kubilay et al., 2000). Anomalous northerly flow over the Red Sea and the west coast of the Arabian Peninsula (and a weaker wind speed) and anomalous southerly flow (and a stronger wind speed) over the eastern Peninsula also suggest a transport of dust from the source regions in the middle and southern Arabian Peninsula, e.g., An Nafud and Ad Dahna deserts, dry riverbeds such as Al Batin, Al-Rimah, and Al Sahba and Rub's al Khali Sandy desert in Saudi Arabia (Ginoux et al., 2012). An Nafud and Ad Dahna deserts are major sources of dust storms in Saudi Arabian in spring to early summer (Notaro et al., 2013) and can also be an important source for Syrian DOD. A modeling study on the sources of spring DOD in Syria also confirms that North Africa (including Libya, Algeria, and Egypt) is the largest source with the secondary source from the Arabian Peninsula (Iraq and Saudi Arabia), and the overall transported DOD is much higher than local DOD in Syria in spring (Ginoux et al., in preparation).

Variations of surface wind associated with the PDO are different from that associated with high DOD, with nearly opposite pattern of cubic wind speeds over the Arabian Peninsula (Figs. 6a and c). When the PDO is positive, anomalous northerly winds pass through the Mediterranean Sea and turn into westerly over the northeastern Africa, which may bring dust

388 from Africa to Israel, Jordan, and Syria as well as increase the moisture transport from the
389 Mediterranean Sea (Fig. 6a). The anomalous southerly wind from the Red Sea also brings
390 moisture onto Syria and tends to promote precipitation. Over southwestern Syria, the anomalous
391 southerly wind is from the less dusty area over northwestern Saudi Arabia and is less likely to
392 enhance Syrian DOD. A weak anomalously westerly flow over the northeastern Saudi Arabia
393 around 30°N and 45°E tends to block the northward transport of dust from the southern and
394 middle Arabian Peninsula to Syria. This westerly flow weakens if extending the time period of
395 regression to 1979 (Fig. 6c). A stronger anomalously westerly flow along the west coast of Saudi
396 Arabia and a southerly flow from the south coast of the Arabian Peninsula are also found in
397 association with the positive PDO during 1979-2015, bringing moisture onto Syria. The
398 discrepancies between the regression patterns in the recent decade and those during 1979-2015,
399 e.g., over the eastern Mediterranean Sea (Figs. 6a and c), are likely associated with the decadal
400 variations of the PDO, indicating an instable connection between the PDO and surface winds in
401 some areas.

402 The anomalous precipitation pattern correlated with the PDO and DOD indices are shown
403 in Figure 7. The PDO has a mild connection with precipitation over the Middle East in spring on
404 the interannual time scale. Similar correlation patterns are found in previous studies that
405 correlated the PDO with low-frequency (i.e., >7years) variations of precipitation (e.g., Dai, 2013,
406 Fig. 2c). A positive phase of the PDO is associated with increased precipitation over most area of
407 the Arabian Peninsula, Turkey, western Iran, and northeastern Africa over Libya and Egypt in
408 the recent decade and during 1948-2015 (Figs. 7a and c). Patterns are similar during 1979-2015
409 (not shown). On the other hand, high DOD in Syria is associated with reduced precipitation over
410 the Arabian Peninsula (particularly, Iraq, central and southern Saudi Arabia), Egypt, eastern

411 Algeria, and western Libya. This is consistent with Fig. 6, which indicates dust transport from
412 these areas to Syria in the spring.

413 Figure 8 shows the vertically integrated mass-weighted moisture flux (vector) and its
414 magnitude (shading) onto the standardized PDO and DOD indices in MAM from 2003-2015 and
415 also onto the standardized PDO index during 1948-2015. Consistent with the precipitation
416 regression patterns (Fig. 7), anomalous anticyclonic moisture flux brings more moisture onto the
417 Arabian Peninsula from the Red Sea and Gulf of Aden associated with a positive PDO (Figs. 8a
418 and c). Moisture flux over the northeastern Africa is also enhanced. Oppositely, high DOD in
419 Syria is associated with an anomalous cyclonic flux centered over the south coast of the Arabian
420 Peninsula, which reduces moisture flux onto the southern Arabian Peninsula (Figs. 8b and d).
421 Moisture flux over northeastern Africa is also reduced associated with an anomalous cyclonic
422 flow over Sudan and Egypt. The pattern of the anomalous moisture fluxes associated with PDO
423 and DOD indices are quite similar to that of the 850 hPa winds (e.g., Fig 5), indicating a
424 dominant role played by low-level moisture transport.

425 These anomalous circulation and moisture flux patterns are also linked to the stability of
426 lower atmosphere. Figure 9 shows the regression of low-level Moist Static Energy (MSE;
427 integrated from surface to 700 hPa) onto the standardized PDO and DOD indices. MSE is
428 defined as a sum of sensible, latent, and geopotential energy in a column air, i.e., $MSE = c_pT+Lq+gz$, where c_p is the specific heat of air at constant pressure, T is air temperature, L is the
429
430 latent heat of vaporization of water, q is specific humidity, and g is the gravity acceleration, and z
431 geopotential height. MSE increasing with altitude denotes a stable atmosphere, so high MSE in
432 the lower atmosphere indicates an instable condition, and vice versa. The patterns of the
433 anomalous MSE are tied to the changes of moisture flux and precipitation anomalies. Reduced

MSE is located over large areas of the Arabian Peninsula, particularly, the southwest coast, in association with high DOD in Syria, indicating a more stable low-level atmosphere and thus less precipitation (Fig. 9b and d). Such a low MSE is also found over North Africa, but in a weaker magnitude. The pattern associated with a positive PDO is nearly opposite, with increased low-level MSE over the Arabian Peninsula, Red Sea, and along the east coast Egypt, denoting an instable atmosphere associated with anomalous moisture transport (Figs. 8a and c) and promoting convection and precipitation (Figs. 9a and c).

In short, Figs. 4-9 show spring circulation and precipitation patterns favorable to high DOD in Syria. Anomalous low pressure over Europe, the southern Arabian Peninsula, and northeastern to eastern Africa promotes westerly winds from North Africa and southerly flow over the southeastern Arabian Peninsula, both of which tend to transport dust to Syria. The anomalous moisture fluxes associated with the geopotential height and wind anomalies also favor a dry and stable condition over the dust source regions adjacent to Syria, such as Saudi Arabia, Iraq, and North Africa. The circulation and precipitation patterns associated with a positive PDO are largely opposite to those associated with high DOD in Syria in the recent decade, which explains the strong negative correlation between the two. Examination on circulation and precipitation variations associated with the PDO in a longer time period (either from 1979-2015 or 1948-2015) show generally similar patterns, but also with some discrepancies. If the conditions associated with high DOD in Syria are valid beyond the recent decade, i.e., 2003-2015, the negative role of the PDO on spring dust activities in Syria is also likely to persist.

5. Analysis on strong dust storms in spring

457 Severe dust storms usually only persist a few days or even a few hours (e.g., Haboobs)
458 and seasonal or monthly averages reduce the variability of dust activities and may smooth out
459 some important features. In this section we discuss the conditions associated with strong dust
460 storms in Syria using daily DOD and reanalysis variables and compare these conditions with
461 those from seasonal mean patterns discussed above including the teleconnections with the PDO.
462 Composites are formed based on daily Syrian DOD index from Aqua. Days during March, April,
463 and May from 2003-2015 are selected when the daily anomaly (with reference to long-term
464 mean) of DOD index is greater than 1 standard deviation to form daily composites. Results are
465 very similar but patterns are in slightly stronger (weaker) magnitudes if choosing the threshold of
466 1.5 (0.5) standard deviations (not shown).
467 Figure 10 shows the composite of Aqua and Terra daily DOD (shading) and ERA-Interim
468 10 m winds based on the Aqua DOD index. The patterns are quite similar in Aqua and Terra
469 DODs. DOD anomaly is above 0.3 over Syria and western Iraq (Figs. 10a-b). Anomalous high
470 DOD is also located over eastern Saudi Arabia and the northeastern Africa, indicating a possible
471 transport of dust from these areas to Syria. Anomalous cyclonic flow is centered over southern
472 Turkey around 30°E, with anomalous strong westerly wind blowing from North Africa and
473 southerly flow from the eastern Arabian Peninsula, consistent with dust transport discussed in the
474 above section. However, different from the seasonal mean regression patterns (e.g., Fig. 6), there
475 are the anomalous southerly winds from the Red Sea and Persian Gulf.
476 Figure 11 shows the composite of daily precipitation from ERA-Interim two times daily
477 forecast and TRMM daily precipitation for days with DOD anomaly above 1 standard deviation.
478 Precipitation anomalies are shown in percentages (with reference to the climatological mean)
479 instead of absolute values in order to highlight the precipitation variations over the Middle East,

where the magnitude of precipitation in spring is quite low (less than 1 mm day^{-1} in most of the areas). Patterns of precipitation anomalies associated with strong dust storms are quite similar in the ERA-Interim and TRMM, but with greater magnitudes in the ERA-Interim. Precipitation increases significantly (about 80% in TRMM and more than 100% in the ERA-Interim) over Turkey and the northeastern Mediterranean, but decreases over the central and southern Arabian Peninsula and northeastern Africa. Syria sits in between the anomalous wet and dry regions, with slightly increased precipitation in its northern domain. These features are somewhat similar to the results of previous studies on strong dust storms and our understanding on the seasonal mean patterns associated with high DOD in Syria. Strong dust storms such as Haboobs (usually about 1 kilometer height and tens to hundreds of kilometer length) are usually associated with convective storms (e.g., Miller et al., 2008; Roberts and Knippertz, 2012; Vukovic et al., 2014; Dempsey, 2014). The cold downdraughts from convective storms spread out and can lift the dust from the surface to form a dusty towering "wall" as the front of a Haboob. Similarly, severe precipitation and convection in Turkey and northern Syria can produce an unstable atmospheric condition in the region, and the intensified low-level winds can lift dust from the surface and thus increase DOD. Reduced precipitation over southern Arabian Peninsula and North Africa facilitates dust transport from these source areas to Syria.

Figure 12 shows composites for vertically integrated mass weighted moisture flux (vectors) and its magnitude (shading) from the NCEP1 and convective available potential energy (CAPE) from the ERA-Interim for days with Aqua DOD ~~index~~ anomaly greater than 1 standard deviation. Fig. 12a shows anomalous westerly flux from northern Egypt and southerly flux from the Red Sea and Persian Gulf largely increase the moisture transport to Syria and eastern Turkey, while the reduced moisture fluxes along the south coast of Iran, southern Arabian Peninsula,

503 southern Red Sea, and the Gulf of Aden are quite similar to those patterns association with high
504 Syrian DOD in spring (Figs. 8b and d) and a negative PDO (i.e., opposite to Fig. 8c).
505 Consistently, CAPE is increased over Turkey and Syria, indicating an unstable atmospheric
506 condition associated with increased moisture transport to the region, while over southern Arabian
507 Peninsula and northeastern Africa where moisture flux is reduced CAPE is decreased (Fig. 12b).
508 The connection between the PDO and daily strong dust storms is also verified by
509 correlating an index of the occurrence of strong dusty events (i.e., daily DOD anomaly greater
510 than 1 standard deviation) in MAM with HadISST from 2003-2015 (supplementary Figure S5).
511 Figs. 10-12 suggest that severe dust storms occur under both favorable large-scale and
512 regional-scale features. Remote forcing such as PDO modifies springtime circulation and
513 precipitation patterns, e.g., a negative phase of PDO decreases precipitation over the southern
514 Arabian Peninsula, northeastern Africa and favors the transport of dry dusty air from these
515 regions to Syria, while strong convective storms over Turkey favor the dust lifting and formation
516 of strong dust storms in Syria.
517
518 **6. Can the recent GFDL climate model capture the connection between the PDO and**
519 **Syrian DOD?**
520 To what extent can current climate model capture the connection between the PDO and
521 Syrian DOD? We examined such relationships in the GFDL AM3 model. Figure 13a shows the
522 correlation between modeled DOD index and surface temperature from 1960-2010 in MAM. The
523 correlation pattern over the North Pacific is quite similar to that of a negative PDO (e.g., Fig. 3c),
524 but only significant over the northern North Pacific, indicting a weaker such connection in the
525 model. Over land, DOD is highly positively associated with surface temperature in the northern

526 to northeastern Africa, which is not seen in the observations, and may suggest an overestimation
527 of the connection in the model. The correlation pattern is similar if calculated from 1951 to 2010,
528 but with a slightly stronger positive correlation over the tropical eastern Pacific (not shown).
529 Fig. 13b shows the regression of standardized DOD index onto 200 hPa (contours) and
530 850 hPa geopotential heights (shading) during MAM 1960-2010. The wave trains propagation
531 from north Pacific to the Middle East is quite similar to that shown in the NCEP1 using observed
532 DOD index (Figs. 4b and d) but in a weaker magnitude in the tropical and subtropical North
533 Pacific, consistent with the weak SST correlations (Fig. 13a). The anomalous low over Africa
534 dips down to the eastern Sahel, probably in association with the biased correlation between the
535 DOD and surface temperature over the northeastern Africa.
536 Figure 13 suggests that AM3 can partially capture the connection between the dust
537 activities in Syria and the PDO during 1960-2010. This complements our satellite observation-
538 based analysis on their relationship in the recent decade, although the modeled relationship is
539 weaker than that in the observations. A few reasons may contribute to this underestimation. First,
540 AOD is slightly underestimated in the Middle East in the model compared with AERONET, and
541 the simulated DOD is also less than that in MODIS, which indicates that dust variability may be
542 underestimated in the region. Second, c~~C~~urrent dust scheme in AM3 only relates dust emission
543 to dust source map and surface wind speed, while the influence of soil moisture on dust emission
544 is not explicitly considered. Thus, the anomalous dust transport from southern Arabian Peninsula
545 and northeast Africa in association with the dry conditions under a negative PDO may not be
546 fully captured by the model. Our analysis also suggest that the DOD in the model is highly
547 correlated with dry deposition over the western Mediterranean, along the north coast of Egypt,
548 and Turkey and with the southwesterly winds in these region, indicating an very strong

connection with the dust sources in Africa, which may be an overestimation. However, it is not uncommon that global or regional climate models have difficulties capturing the interannual to decadal variations of dust aerosols (e.g., Evan et al., 2014; Solmon et al. 2015). This is why we did not choose the climate model as a major tool to examine the connection between the PDO and Syrian DOD in this work. A new dust emission scheme that considers the influences of soil moisture and vegetation cover and land use changes is currently under development, and the relationship between Syrian DOD and PDO is likely to be better represented in this newer version of the GFDL model.

7. Conclusions

Dust activities in the Middle East have been related to a lot factors, such as remote sea surface temperatures, near surface winds, vegetation coverage, and precipitation variability. The ongoing civil war and a recent severe dust storm in Syria in 2015 raised concerns as whether dust activities will increase in the region. First step toward answering this question is to understand the dust activities driven by the natural climate variability. Here we examine the connection between Syrian dust activities and the Pacific decadal oscillation (PDO) using innovative dust optical depth (DOD) datasets retrieved from MODIS Deep Blue aerosol products and multiple observations and reanalyses.

A significantly negative correlation is found between Syrian DOD and the PDO in springtime during 2003-2015, suggesting that the PDO index explains about 81% variances of Syrian DOD in spring in the recent decade. Such a connection is revealed not only on precipitation as emphasized by previous studies (e.g., Yu et al., 2014; Notaro et al., 2015) but also on other aspects such as the circulation patterns and surface winds. It is found that high

572 DOD in Syria during spring is associated with low geopotential height over Europe, southern
573 Arabian Peninsula, and northeastern to eastern Africa. Associated with these anomalous height
574 patterns are the westerly wind anomalies over the Mediterranean basin and southerly wind
575 anomalies over the southeastern Arabian Peninsula, favoring dust transport from these regions to
576 Syria, where the transported dust dominates the DOD in spring (Ginoux et al., in preparation). A
577 positive PDO is connected with wind and height patterns largely opposite to those associated
578 with high DOD over Syria. Positive phase of the PDO also tends to increase precipitation over
579 the Arabian Peninsula and northeastern Africa via anomalous moisture transport that increases
580 moisture supply and also reduces the stability of low-level atmosphere. A negative PDO thus is
581 not only associated with wind and geopotential height patterns favorable to high DOD in Syria
582 but also tends to reduces precipitation in the dust source regions such as Iraq, Saudi Arabia, and
583 northeastern Africa, and thus favors dust transport to Syria. This explains why the correlation
584 between the Syrian DOD index and the PDO index is much higher than other individual index
585 such as precipitation, leaf area index, and 10 m winds in Syria (Tables 1-2). The influences of the
586 PDO on circulation and precipitation patterns over the Middle East largely persist beyond the
587 recent decade, ~~i.e~~e.g., over 1948-2015, but also show some exceptions. The lack of long-term
588 observations also brings uncertainties to the connection between the PDO and Syrian DOD.
589 Different from the patterns on seasonal mean discussed above, analysis on the daily
590 composites of strong spring dust storms shows both the influence of the PDO and local features.
591 In spring, strong dust storms (DOD anomalies greater than 1 standard deviation) in Syria is
592 associated with an anomalous cyclonic flow centered over the northeastern Mediterranean Sea
593 and Turkey, and southerly wind anomalies from the Red Sea and Persian Gulf. Consistently,
594 moisture flux onto Turkey and Syria is enhanced and thus destabilizes the atmosphere and

promotes precipitation in Turkey and convection and dust uplifting in Syria. Meanwhile, reduced moisture fluxes onto the southern Arabian Peninsula and east coast of Egypt and Sudan in association with a negative PDO favor a dry and stable condition in Saudi Arabia and northeastern Africa, facilitating dust transport from these regions to Syria.

We examined the teleconnection between ~~the~~ Syrian DOD and the PDO in the GFDL AM3 model. A weaker connection compared to that in the observation is found, which may be partially related to model's underestimation of the mean DOD and its variability in this area. The new dust scheme that includes the influence of soil moisture and precipitation is likely to overcome these drawbacks and provide a better representation of the relationship between Syrian DOD and the PDO.

Acknowledgements.

PRECL Precipitation data is provided by the NOAA/OAR/ESRL PSD, Boulder, Colorado, USA, from their Web site at http://www.esrl.noaa.gov/psd/. PDO and Niño3.4 indices are downloaded from the website of NOAA Climate Prediction Center (http://www.esrl.noaa.gov/psd/data/climateindices/list/). The NCEP/NCAR reanalysis product was obtained from http://www.esrl.noaa.gov/psd/data/gridded/data.ncep.reanalysis.html and the ERA-Interim is downloaded from http://www.ecmwf.int/en/research/climate-reanalysis/era-interim. HadISST is downloaded from http://www.metoffice.gov.uk/hadobs/hadisst/data/download.html while CRU TS 3.23 temperature and precipitation are downloaded from https://crudata.uea.ac.uk/cru/data/hrg/cru_ts_3.23/cruts.1506241137.v3.23/. The MODIS Deep Blue aerosol products were acquired from the Level-1 and Atmosphere Archive and Distribution System (LAADS) Distributed Active Archive Center (DAAC), located in the Goddard Space Flight Center in Greenbelt, Maryland (https://ladsweb.nascom.nasa.gov/). This research was supported by NOAA and Princeton University's Cooperative Institute for Climate Science and NASA under grants NNG14HH42I-MAP and NNH14ZDA001N-ACMAP.

641 Reference

642 Alexander, M. A., Bladé, I., Newman, M., Lanzante, J. R. , Lau, N.-C., and Scott, J. D. : The
643 atmospheric bridge: The influence of ENSO teleconnections on air–sea interaction over
644 the global oceans.J. Climate, 15, 2205–2231, 2002.
645 Anderson, T. L., Wu, Y., Chu, D. A., Schmid, B., Redemann, J., and Dubovik, O.: Testing the
646 MODIS satellite retrieval of aerosol fine-mode fraction, *J. Geophys. Res*., 110, D18204,
647 doi: 10.1029/2005JD005978, 2005.
648 Banerjee, P, and Kumar, S. P.: ENSO modulation of interannual variability of dust aerosols over
649 the northwest Indian Ocean, J. Climate, 29,1287-1303, 2016.
650 Bangert, M., Nenes, A., Vogel, B., Vogel, H., Barahona, D., Karydis, V. A., Kumar, P.,
651 Kottmeier, C., and Blahak, U.: Saharan dust event impacts on cloud formation and
652 radiation over Western Europe, Atmos. Chem. Phys., 12, 4045–4063, 2012.
653 Barlow, M., Cullen, H., and Lyon, B. : Drought in central and southwest Asia: La Niña, the
654 warm pool, and Indian Ocean precipitation. J. Climate, 15, 697–700, doi:10.1175/1520-
655 0442(2002)015,0697:DICASA.2.0.CO;2, 2002.
656 Chen, M., Xie, P., Janowiak, J. E. and Arkin, P. A.: Global Land Precipitation: A 50-yr Monthly
657 Analysis Based on Gauge Observations, J. of Hydrometeorology, 3, 249-266, 2002.
658 Chin, M., et al.: Multi-decadal aerosol variations from 1980 to 2009: A perspective from
659 observations and a global model, Atmos. Chem. Phys., 14, 3657–3690, 2014.
660 Choobari, O. A., Zawar-Reza, P., and turman, A.: The global distribution of mineral dust and its
661 impacts on the climate system: A review, Atmospheric Research, 138, 152-165, 2014.
662 Claverie, M., Vermote E., and NOAA CDR Program: NOAA Climate Data Record (CDR) of
663 Leaf Area Index (LAI) and Fraction of Absorbed Photosynthetically Active Radiation

(FAPAR), Version 4. [indicate subset used]. NOAA National Climatic Data Center. doi:10.7289/V5M043BX [access date], 2014.

Claverie, M., Matthews, J. L., Vermote, E. F., and Justice, C. O.: A 30+ year AVHRR LAI and FAPAR climate data record: Algorithm description and validation, Remote Sens., 8, 263; doi:10.3390/rs8030263, 2016.

Dai, A.: The influence of the inter-decadal Pacific oscillation on US precipitation during 1923-2010, Clim. Dyn., 41, 633-646.doi: 10.1007/s00382-012-1446-5, 2013.

D'Almeida, G. A.: Desert aerosol characteristics and effects on climate. In Palleoclimatology and Paleometeorology: Modern and Past patterns of Global Atmospheric Transport. Lienen M., Sarnthein M. (eds). Kluwer Academic Publishers, 311-338, 1987.

Dayan: Climatology of back trajectories from Israel based synoptic analysis, Journal of Climate and Applied Meteorology, 25, 591-595, 1986.

Dayan, U., Ziv, B., Shoob, T., and Enzel, Y. : Suspended dust over southeastern Mediterranean and its relation to atmospheric circultions, Int. J. of Climatol., 28, 915-924, 2008.

Dayan, U., Tubi, A., and Levy, I.: On the importance of synoptic classification methods with respect to environmental phenomena, Int. J. of Climatol., 32, 681-694, 2012.

Dee, D. P. et al.: The ERA-Interim reanalysis: configuration and performance of the data assimilation system, Q.J.R. Meteorol. Soc., Vol. 137: 553-597, DOI: 10.1002/qj.828, 2011

Dempsey, M. J.: Forecasting strategies for Haboobs: an underreported weather phenomenon, Advances in Meteorology, http://dx.doi.org/10.1155/2014/904759, 2014.

Deser, C., and Blackmon, M. L.: On the relationship between tropical and North Pacific sea surface temperature variations. J. Climate, 8, 1677–1680, 1995.

687 Donner, L., Wyman, B. L., Hemlert, R. S. and et al.: The dynamical core, physical
688 parameterizations, and basic simulation characteristics of the atmospheric component
689 AM3 of the GFDL global coupled model CM3, J. Climate, 24, 3484-3519, 2011.
690 Eck, T. F., Holben, B. N., Reid, J. S., Dubovik, O., Smirnov, A., O'Neill, N. T., Slutsker, I.,
691 Kinne, S.: Wavelength dependence of the optical depth of biomass burning, urban, and
692 desert dust aerosols, J. Geophys. Res., 104(D24), 31333-31349, 1999.
693 Evan, A. T., Flamant, C., Fiedler, S., and Doherty, O.: An analysis of aeolian dust in climate
694 models, Geophys. Res. Lett., 41, 5996–6001, doi:10.1002/2014GL060545, 2014.
695 Evans, M. N., Cane, M. A., Schrag, D. P. , Kaplan, A., Linsley, B. K., Villalba, R., and
696 Wellington, G. M.: Support for tropically-driven Pacific decadal variability based on
697 paleoproxy evidence, Geophys. Res. Lett., 28, 3689-3691, 2001.
698 Fung, I., Meyn, S., Tegen, I., Doney, S. C., John, J., and Bishop, J. K. B. : Iron supply and
699 demand in the upper ocean, Global Biogeochem. Cycle, 14, 281–296, 2000.
700 Ginoux, P., Chin, M., Tegen, I., Prospero, J. M., Holben, B., Dubovik, O., and Lin, S.-J.: Sources
701 and distributions of dust aerosols simulated with the GOCART model. J. Geophys. Res.,
702 106, 22 255–22 274, 2001.
703 Ginoux, P., Prospero, J. M., Gill, T. E., Hsu, N. C., and Zhao, M.: Global-scale attribution of
704 anthropogenic and natural dust sources and their emission rates based on the MODIS
705 Deep Blue aerosol products, Rev. Geophys., 50, RG3005, 2012.
706 Ginoux, P., Prospero, J, M., Torres, O., and Chin, M.: Long-term simulation of global dust
707 distribution with the GOCART model: Correlation with North Atlantic Oscillation,
708 Environ. Model. Software, 19, 113-128, doi:10.1016/S1364-8152(03)00114-2, 2004.

709 Harris, I., Jones, P.D., Osborn, T.J. and Lister, D.H.: Updated high-resolution grids of monthly
710 climatic observations –the CRU TS3.10 Dataset. Int. J. Climatol., 34:623–642.
711 doi:10.1002/joc.3711, 2014.
712 Hsu, N. C., Tsay, S.-C., King, M., and Herman, J. R.: Aerosol properties over bright-reflecting
713 source regions, IEEE Trans. Geosci. Remote Sens., 42, 577-569, 2004.
714 Hsu, N. C., Tsay, S.-C. , King, M., and Herman, J. R.: Deep blue retrievals of Asian aerosol
715 properties during ACE-Asia, IEEE Trans. Geosci. Remote Sens., 44, 3180-3195, 2006.
716 Huang, B., Banzon, V.F., Freeman, E., Lawrimore, J., Liu, W., Peterson, T.C., Smith, T.M.,
717 Thorne, P.W., Woodruff, S.D., and Zhang, H.-M.: Extended Reconstructed Sea Surface
718 Temperature version 4 (ERSST.v4): Part I. Upgrades and intercomparisons. *Journal of*
719 *Climate*, 28, 911-930, doi:10.1175/JCLI-D-14-00006.1, 2015.
720 Huang, B., Thorne, P., Smith, T., Liu, W., Lawrimore, J., Banzon, V., Zhang, H., Peterson, T.,
721 and Menne, M.: Further Exploring and Quantifying Uncertainties for Extended
722 Reconstructed Sea Surface Temperature (ERSST) Version 4 (v4). *Journal of Climate,* 29,
723 3119-3142, doi:10.1175/JCLI-D-15-0430.1, 2016.
724 Huang, J., Wang, T., Wang, W., Li, Z., and Yan, H.: Climate effects of dust aerosol over East
725 Asian arid and semiarid regions, J. Geophys. Res. Atmos., 119, 11,398-11,416,
726 doi:10.1002/2014JD21796, 2014.
727 Huffman, G. J., and Bolvin, D.T.: TRMM and other data precipitation data set documentation.
728 TRMM Doc., 42 pp. [Available online at ftp:// meso-a.gsfc.nasa.gov/pub/
729 trmmdocs/3B42 _3B43_doc.pdf.], 2014

730 Israelevich, P. L., Ganor, E., Levin, Z., and Joseph, J. H.: Annual variations of physical
731 properties of desert dust over Israel, J. Geophys. Res., 180(D13), 4381, doi:
732 10.1029/2002JD003163, 2003.
733 Jin, Q., Wei, J., and Yang, Z.-L.: Positive response of indian summer rainfall to middle east dust,
734 Geophys. Res. Lett., 41 (11), 4068–4074, doi:10.1002/2014gl059980, 2014.
735 Jin, Q., Wei, J., Yang, Z.-L., Pu, B., and Huang, J.-P.: Consistent response of indian summer
736 monsoon to middle east dust in observations and simulations, Atmospheric Chemistry
737 and Physics, 15 (17), 9897–9915, doi:10.5194/acp-15-9897-2015, 2015.
738 Jin, Q., Yang, Z.-L., and Wei, J.: Seasonal Responses of Indian Summer Monsoon to Dust
739 Aerosols in the Middle East, India, and China. J. Climate. doi:10.1175/JCLI-D-15-
740 0622.1, in press, 2016.
741 Kalnay, E., et al.: The NCEP/NCAR 40-year reanalysis project, Bull. Am. Meteorol. Soc., 77(3),
742 437–471, doi:10.1175/1520-0477(1996)077<0437:Tnyrp>2.0.Co;2, 1996.
743 Kim, M.-K., Lau, W. K. M., Kim, K.-M., Sang, J., Kim, Y.-H., and Lee, W.-S.: Amplification of
744 ENSO effects on Indian summer monsoon by absorbing aerosols, Clim. Dyn., 46, 2657-
745 2671, 2016.
746 Klingmüller, K., Pozzer, A., Metzger, S., Stenchikov, G., and Lelieveld, J.: Aerosol optical depth
747 trend over the Middle East, Atmos. Chem. Phys., 16, 5063-5073, 2016.
748 Kubilay, N., Nickovic, S., Moulin, C., and Dulac, F.: An illustration of the transport and
749 deposition of mineral dust onto the eastern Mediterranean. Atmos. Environ., 34, 1293–
750 1303, doi:10.1016/S1352-2310(99)00179-X, 2000.

751 Lau, K. M., Kim, K. M., Sud, Y. C., and Walker, G. K.: AGCM study of the response of the
752 atmospheric water cycle of West Africa and the Atlantic to Saharan dust radiative
753 forcing. Ann. Geophys., 27, 4023–4037, doi:10.5194/angeo-27-4023-2009, 2009.
754 Levin, Z., Ganor, E., and Gladstein, V.: The effects of desert particles coated with sulfate on rain
755 formation in the eastern Mediterranean. J. Appl. Meteor., 35, 1511–1523, doi:10.1175/
756 1520-0450(1996)035,1511:TEODPC.2.0.CO;2, 1996.
757 Li, F., Ginoux, P., and Ramaswamy, V.: Distribution, transport, and deposition of mineral dust in
758 the Southern Ocean and Antarctica: Contribution of major sources, J. Geophys. Res.,
759 113: D10207, doi:10.1029/2007JD009190, 2008.
760 Lin, S.-J.: A finite-volume integration method for computing pressure-gradient force in general
761 vertical coordinates. Quart. J. Roy. Meteor. Soc., 123, 1749–1762, 1997.
762 Lin, S.-J.: A ‘‘vertically Lagrangian’’ finite-volume dynamical core for global models. Mon.
763 Wea. Rev., 132, 2293–2307, 2004.
764 Lin, S.-J., , and Rood, R. B.: Multidimensional flux-form semi- Lagrangian transport schemes.
765 Mon. Wea. Rev., 124, 2046–2070, 1996.
766 Lin, S.-J., and Rood, R. B.: An explicit flux-form semi-Lagrangian shallow water model on the
767 sphere. Quart. J. Roy. Meteor. Soc., 123, 2477–2498, 1997.
768 Liu, Z., and Alexander, M.: Atmospheric bridge, oceanic tunnel, and global climatic
769 teleconnections. Rev. Geophys., 45, RG2005, doi:10.1029/2005RG000172, 2007.
770 Liu, W., Huang, B., Thorne, P.W., Banzon, V.F., Zhang, H.-M., Freeman, E., Lawrimore, J.,
771 Peterson, T.C., Smith, T.M., and Woodruff, S.D.: Extended Reconstructed Sea Surface
772 Temperature version 4 (ERSST.v4): Part II. Parametric and structural uncertainty
773 estimations. *Journal of Climate*, 28, 931-951, doi:10.1175/JCLI-D-14-00007.1, 2015.

774 Mahowald, N. M., and Coauthors: Observed 20th century desert dust variability: Impact on
775 climate and biogeochemistry. Atmos. Chem. Phys., 10, 10 875–10 893, doi:10.5194/acp-
776 10-10875-2010, 2010.
777 Mantua, H., and Hare, S. R.: The Pacific Decadal Oscillation, J. of Oceanography, 58, 35-44,
778 2002.
779 Mariotti, A.: How ENSO impacts precipitation in southwest central Asia. Geophys. Res. Lett.,
780 34, L16706, doi:10.1029/ 2007GL030078, 2007.
781 Mariotti, A., Ballabrera-Poy, J., and Zeng, N.: Tropical influence on Euro-Asian autumn rainfall
782 variability. Climate Dyn., 24, 511–521, doi:10.1007/s00382-004-0498-6, 2005.
783 Miller, R. L, and Tegen, I.: Climate response to soil dust aerosols. J. Climate, 11, 3247–3267,
784 doi:10.1175/1520-0442(1998)011,3247: CRTSDA.2.0.CO;2, 1998.
785 Miller, R. L, Tegen, I., and Perlwitz, J.: Surface radiative forcing by soil dust aerosols and the
786 hydrologic cycle. J. Geophys. Res., 109, D04203, doi:10.1029/2003JD004085, 2004.
787 Miller, S., Kuciauskas, A. P., Liu, M., Ji, Q., Reid, J.S., Breed, D. W. , Walker, A. L., and
788 Mandoos, A. A.: Haboob dust storms of the southern Arabian Peninsula, J. Geophys.
789 Res., 113, D01202, doi:10.1029/2007JD008550, 2008.
790 Mills, C. M., and Walsh, J. E.: Seasonal variation and spatial patterns of the atmospheric
791 component of the Pacific decadal oscillation, J. Climate, 26, 1575-1594, 2013.
792 Minobe, S.: A 50-70 year climate oscillation over the North Pacific and North America,
793 Geophys. Res. Lett., 24, 683-686, 1997.
794 Moorthi, S. and Suarez, M. J.: Relaxed Arakawa-Schubert. A parameterization on moist
795 convection for general circulation models, Mon. Weather Rev., 120, 978-1002, 1992.

796 Morman, S. A., and Plumlee, G. S.: The role of airborne mineral dusts in human disease, Aeolian
797 Research, 9, 203-212, doi:10.1016/j.aeolia.2012.12.001.,2013.
798 Moulin, C., Lambert, C. E., Dulac, F., Dayan, U.: Control of atmospheric export of dust from
799 North Africa by the North Atlantic oscillation. Nature, 387, 691-694, 1997.
800 Nakajima, T., Higurashi, A., Kawamoto, K., and Penner, J. E.: A possible correlation between
801 satellite-derived cloud and aerosol microphysical parameters, Geophys. Res. Lett., 28,
802 1171–1174, doi:10.1029/2000GL012186, 2001.
803 Newman, M., Compo, G. P. and Alexander, M.: ENSO-forced variability of the Pacific decadal
804 oscillation, J. Climate, 16, 3853-3857, 2003.
805 Notaro, M., Alkolibi, F., Fadda, E., and Bakhrjy, F.: Trajectory analysis of Saudi Arabian dust
806 storms, J. Geophys. Res. Atmos., 118, 6028–6043.Notaro, M., Y. Yu, and O. V.
807 Kalashnikova (2015), Regime shift in Arabian dust activity, triggered by persistent
808 Fertile Crescent drought, J. Geophys. Res. Atmos., 120, 10,229–10,249,
809 doi:10.1002/2015JD023855, 2013.
810 Pozzer, A., de Meij, A., Yoon, J., Tost, H., Georgoulias, A. K., and Astitha, M.: AOD trends
811 during 2001–2010 from observations and model simulations, Atmos. Chem. Phys., 15,
812 5521–5535, 2015. doi:10.5194/acp-15-5521-2015.
813 Price, C., Stone, L., Huppert, A., Rajagopalan, B., and Alpert, P.: A possible link between El
814 Niño and precipitation in Israel, Geophys. Res. Lett., 25, 3963–3966,
815 doi:10.1029/1998GL900098, 1998.
816 Rayner, N. A., Parker, D. E., Horton, E. B., Folland, C. K., Alexander, L. V., Rowell, D. P.,
817 Kent, E. C., Kaplan, A.: Global analyses of sea surface temperature, sea ice, and night

818 marine air temperature since the late nineteenth century J. Geophys. Res.Vol. 108, No.
819 D14, 4407 10.1029/2002JD002670, 2003.
820 Roberts, A., and Knippertz, P.: Haboobs: convectively generated dust storms in West Africa,
821 Weather, 67, 311-316, 2012.
822 Rosenfeld, J. E., Considine, D. B., Meade, P. E., Bacmeister, J. T., Jackman, C. H., and
823 Schoeberl, M. R.: Stratospheric effects of Mount Pinatubo aerosol studied with a coupled
824 two-dimensional model, J. Geophys. Res., 102, 3649–3670, doi:10.1029/96JD03820,
825 1997.
826 Schneider, N., and Cornuelle, B.: The forcing of the Pacific decadal oscillation, J. Climate, 18,
827 4355-4373, 2005.
828 Shao, Y.: A model for minderal dust emission, J Geophys. Res., 160(D17), 20, 239-
829 20,254,doi:10.1029/2001JD900171, 2001.
830 Shao, Y., Wyrwoll, K. H., and Cappell, A., et al.: Dust cycle: an emerging core theme in Earth
831 system science. Aeolian Res., 2, 181-204, 2011.
832 Simmons, A. J., and Burridge, D. M.: An energy and angularmomentum conserving vertical
833 finite-difference scheme and hybrid vertical coordinates. Mon. Wea. Rev., 109, 758–766,
834 1981.
835 Solmon, F., Mallet, M., Elguindi, N. Fiorfi, F., Zakey, A., and Konare, A. : Dust aerosol impact
836 on regional precipitation over western Africa, mechanisms and sensitivity to absorption
837 properties. Geophys. Res. Lett., 35, L24705, doi:10.1029/2008GL035900, 2008.
838 Solmon, F., Elguindi, N., and Mallet, M.: Radiative and climatic effects of dust over West
839 Africa, as simulated by a regional climate model. Climate Res., 52, 97–113,
840 doi:10.3354/cr01039, 2012.

841 Solmon, F., Nair, V. S., and Mallet, M.: Increasing Arabian dust activity and the Indian summer
842 monsoon, Atmos. Chem. Phys., 15, 8051–8064, doi:10.5194/acp-15-8051-2015, 2015.
843 Strong, C., and Magnusdottir, G.: The role of tropospheric Rossby wave breaking in the Pacific
844 decadal oscillation, 22, 1819-1833, 2009.
845 Strong, J. D.O., Vecchi, G. A., and Ginoux, P.: The response of the tropical Atlantic and West
846 African climate to Saharan dust in a fully coupled GCM, J. climate, 28, 7071-7092, 2015.
847 Tegen, I., Lacis, A., and Fung, I.: The influence of mineral aerosol from disturbed soils on the
848 global radiation budget, Nature, 380, 419-422, 1996.
849 Vinoj, V., Rasch, P. J., Wang, H. L., Yoon, J. H., Ma, P. L., Landu, K., and Singh, B.: Short-
850 term modulation of Indian summer monsoon rainfall by West Asian dust, Nat. Geosci., 7,
851 308–313, 2014.
852 Vukovi, A., Vujadinovic, M., Pejanovic, G., Andric, J., Kumjian, M. R., Djurdjevic, V., Dacic,
853 M., Prasad, A. K., El-Askary, H. M., Paris, B. C., Petkovic, S., Nickovic, S., and Sprigg,
854 W. A.: Numerical simulation of “an American haboob”, Atmos. Chem, Phys., 14, 3211-
855 3230, 2014.
856 Wang, S., Huang, J., He, Y., and Guan, Y.: Combined effects of the Pacific Decadal Oscillation
857 and El Niño-Southern Oscillation on global land dry-wet changes, Sci. Rep., 4, 6651,
858 doi:10.1038/srep06651, 2014.
859 Wurzler, S. C., Reisin, T. G., and Levin, Z.: Modification of mineral dust particles by cloud
860 processing and subsequent effects on drop size distributions, J. Geophys. Res., 105(D4),
861 4501–4512, doi:10.1029/1999JD900980, 2000.
862 Yoshioka, M., Mahowald, N. M., Conley, A. J., Collins, W. D., Fillmore, D. W., Zender, C. S.,
863 and Coleman, D. B.: Impact of desert dust radiative forcing on Sahel precipitation:

Relative importance of dust compared to sea surface temperature variations, vegetation changes, and greenhouse gas warming. J. Climate, 20, 1445–1467, doi:10.1175/JCLI4056.1, 2007.

Yu, Y., Notaro, M., Liu, Z., Wang, F., Alkolibi, F., Fadda, E., and Bakhrjy, F.: Climatic controls on the interannual to decadal variability in Saudi Arabian dust activity: Toward the development of a seasonal dust prediction model, J. Geophys. Res. Atmos., 120, 1739–1758, 2015.

Yue, X., Wang, H., Liao, H., and Fan, K.: Direct climatic effect of dust aerosol in the NCAR Community Atmosphere Model version 3 (CAM3). Adv. Atmos. Sci., 27, 230–242, doi:10.1007/ s00376-009-8170-z, 2010.

Yue, X., Liao, H., Wang, H. J., Li, S. L., and Tang, J. P.: Role of sea surface temperature responses in simulation of the climatic effect of mineral dust aerosol. Atmos. Chem. Phys., 11, 6049–6062, doi:10.5194/acp-11-6049-2011, 2011.

Zhang, Y., Wallace, J. M., and Battisti, D. S.: ENSO-like interdecadal variability, J. Clim., 10, 1004–1020.Zhang, L., And T. Delworth, 2015: Analysis of the characteristic and mechanisms of the Pacific decadal oscillation in a suite of coupled models from the Geophysical Fluid Dynamics Laboratory, J. Climate, 28, 7678-7701, 1997.

887 Table 1 Correlations between monthly DOD indices and the PDO, Niño3.4 indices, precipitation from the
888 CRU TS3.23 (P1; 2003-2014) and PRECL (P2), AVHRR LAI (LAI1), MODIS Aqua LAI (LAI2) and 10
889 m wind speed from the ERA-Interim averaged over Syria (see the box in Fig.2) for all the month
890 (seasonal cycles are removed) from 2003-2015 (or 2014). Coefficients significant at the 95% confidence
891 level are in bold.
892
893 Table 2 Same as table 1 but for MAM average from 2003-2015 (or 2014). Coefficients significant at the
894 95% confidence level are in bold.
895
896
897
898
899
900
901
902
903
904
905
906
907
908
909
910
911
912

913 Figure 1. Monthly time series of Aqua (green) and Terra (grey) DOD indices averaged over Syria (see
914 Fig. 2 for domain) and PDO index (orange; multiplying by -1 to show its negative connection with the
915 DOD indices).
916
917 Figure 2. Correlation between the PDO index and MODIS (a) Aqua and (b) Terra DOD in MAM from
918 2003-2015. (c) Correlation between Syrian DOD indices (navy and green bar denotes Terra and Aqua,
919 respectively) and PDO index for each month and annual mean (ANN) from 2003 to 2015. Red dashed
920 lines denote the 95% confidence level (t test). Red box denotes the averaging area for Syrian DOD index.
921
922 Figure 3. Correlation between the PDO index and HadISST (over the ocean) and CRU TS3.23 near-
923 surface temperature (over land) for (a) MAM and (b) annual mean during 2003-2014. Correlation
924 between (c)-(d) Aqua and (e)-(f) Terra DOD indices and HadISST and CRU near-surface temperature for
925 (c), (e) MAM and (d), (f) annual mean during 2003-2014. Areas significant at the 95% confidence level
926 (t-test) are dotted.
927
928 Figure 4. Regression of 850 hPa (shading) and 200 hPa (blue contours; solid lines for positive values and
929 dashed lines for negative values, from -40 gpm to 40 gpm with an interval of 10 gpm, zero line is not
930 shown) geopotential heights onto the standardized PDO index for (a) 2003-2015 and (c) 1948-2015 and
931 onto the standardized (b) Aqua and (d) Terra DOD indices. Areas significant at the 95% confidence level
932 (t-test) are dotted.
933
934 Figure 5. Regressions of NCEP1 850 hPa geopotential height (shading; gpm) and horizontal winds
935 (vectors; m s^{-1}) onto the standardized PDO index during (a) 2003-2015 and (c) 1948-2015, and onto the
936 standardized (b) Aqua and (d) Terra DOD indices during 2003-2015. Area where the regression is
937 significant at the 95% confidence level (t-test) is dotted, and vectors significant at the 90% confidence
938 level are plotted in blue.

939 Figure 6. Regressions of ERA-Interim 10 meter horizontal winds (green vectors; m s^{-1}) and cubic wind
940 speed (shading; m^3 s^{-3}) onto standardized PDO index (a) from 2003-2015 and (c) from 1979-2015 and
941 onto the standardized (b) Aqua and (d) Terra DOD indices. Areas where the regressions of the wind speed
942 are significant at the 95% confidence level are dotted and vectors significant at the 90% confidence level
943 are plotted in blue (t-test).
944
945 Figure 7. Correlation between PRECL precipitation and PDO index during (a) 2003-2015, (c) 1948-2015
946 and between precipitation and (b) Aqua and (d) Terra DOD indices during 2003-2015. Areas where the
947 correlation coefficients are significant at the 95% confidence level (t-test) are dotted.
948
949 Figure 8. Regression of vertically integrated mass weighted monthly moisture flux (vectors; kg m^{-1} s^{-1})
950 and its magnitude (shading) onto standardized PDO index during (a) 2003-2015 and (c) 1948-2015, and
951 onto the standardized (b) Aqua and (d) Terra DOD indices. Moisture flux is integrated from surface to
952 300 hPa. Areas with magnitude of moisture flux significant at the 90% confidence level are dotted, and
953 moisture fluxes significant at the 90% confidence level are plotted in purple vectors (t-test).
954
955 Figure 9. Regression of vertically integrated MSE (10^4 J m^{-2}) over the lowest four atmospheric layers
956 (1000, 925, 850, and 700 hPa) from the NCEP1 onto the standardized PDO index for (a) 2003-2015 and
957 (c) 1948-2015 and onto the standardized DOD indices from MODIS (b) Aqua and (d) Terra during 2003-
958 2015. Areas significant at the 90% confidence level (t-test) are dotted.
959
960 Figure 10. Composites of (a) Aqua and (b) Terra daily DOD (shading) along with ERA-Interim 10 m
961 horizontal wind anomalies (with reference to the 1979-2015 mean; vectors) for days with Syrian DOD
962 index (Aqua) greater than 1 standard deviation during MAM from 2003-2015. Shading shows values
963 significant at the 95% confidence level over land, while wind vectors significant at the 95% confidence
964 are plotted in blue (t-test).

965 Figure 11. Composites of daily precipitation anomalies (shading; % with references to the climatology)
966 from (a) the ERA-interim and (b) TRMM for the days with Syrian DOD index (Aqua) greater than 1
967 standard deviation during MAM from 2003-2015. Areas significant at the 95% confidence level (t-test)
968 are dotted.
969
970 Figure 12. Composites of (a) vertically integrated mass-weighted moisture flux (vectors; kg $m^{-1}s^{-1}$) and its
971 magnitude (shading) from the NCEP1 and (b) CAPE (10^4 J/kg) along with 850 hPa winds (m s^{-1}) from the
972 ERA-Interim for the days with Syrian DOD index (Aqua) greater than 1 standard deviation during MAM
973 from 2003-2015. Moisture flux is integrated from surface to 300 hPa. Shading areas significant at the
974 95% confidence level are dotted.
975
976 Figure 13. (a) Correlation between AM3 DOD index averaged over Syria (see Fig. 2) and surface
977 temperature from 1960-2010 and (b) regression of 850 hPa (shading) and 200 hPa (contours; solid lines
978 for positive values and dashed lines for negative values, from -20 gpm to 20 gpm with intervals of 5 gpm,
979 zero line is not shown) geopotential height onto the standardized DOD index from 1960-2010. Shading
980 areas significant at the 95% confidence level are dotted.
981
982
983
984
985
986
987
988
989
990

Table 1 Correlations between monthly DOD indices and the PDO, Niño3.4 indices, precipitation from the CRU TS3.23 (P1; 2003-2014) and PRECL (P2), AVHRR LAI (LAI1), MODIS Aqua LAI (LAI2) and 10 m wind speed from the ERA-Interim averaged over Syria (see the box in Fig.2) for all the month (seasonal cycles are removed) from 2003-2015 (or 2014). Coefficients significant at the 95% confidence level are in bold.

	PDO	Niño3.4	P1	P2	LAI1	LAI2	10 m wind
Aqua DOD	**-0.51**	**-0.24**	-0.05	-0.05	**-0.35**	**-0.41**	-0.00
Terra DOD	**-0.50**	**-0.23**	-0.05	-0.06	**-0.32**	**-0.39**	-0.02

Table 2 Same as table 1 but for MAM average from 2003-2015 (or 2014). Coefficients significant at the 95% confidence level are in bold.

	PDO	Niño3.4	P1	P2	LAI1	LAI2	10 m wind
Aqua DOD	**-0.90**	**-0.60**	-0.14	-0.38	**-0.60**	**-0.64**	0.31
Terra DOD	**-0.90**	**-0.60**	-0.10	-0.34	**-0.57**	**-0.61**	0.30

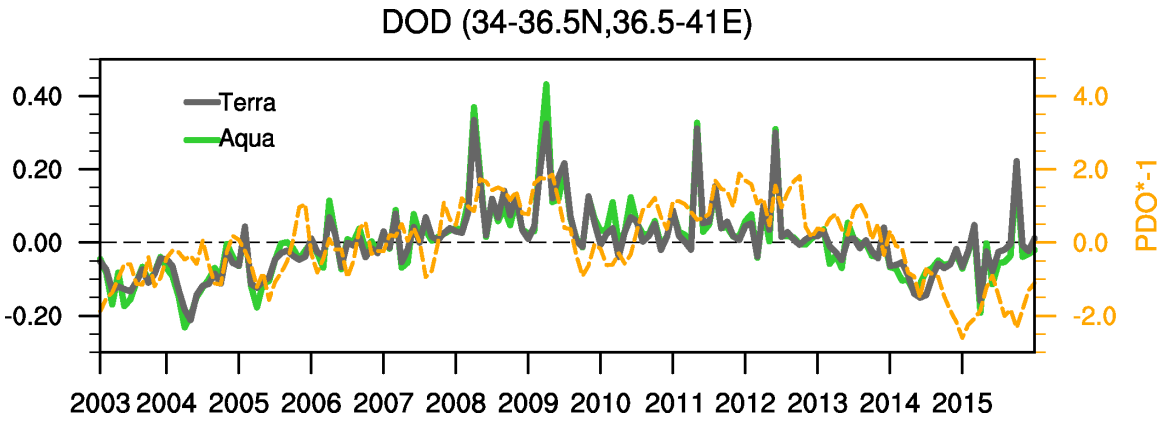

Figure 1. Monthly time series of Aqua (green) and Terra (grey) DOD indices averaged over Syria (see Fig. 2 for domain) and PDO index (orange; multiplying by -1 to show its negative connection with the DOD indices).

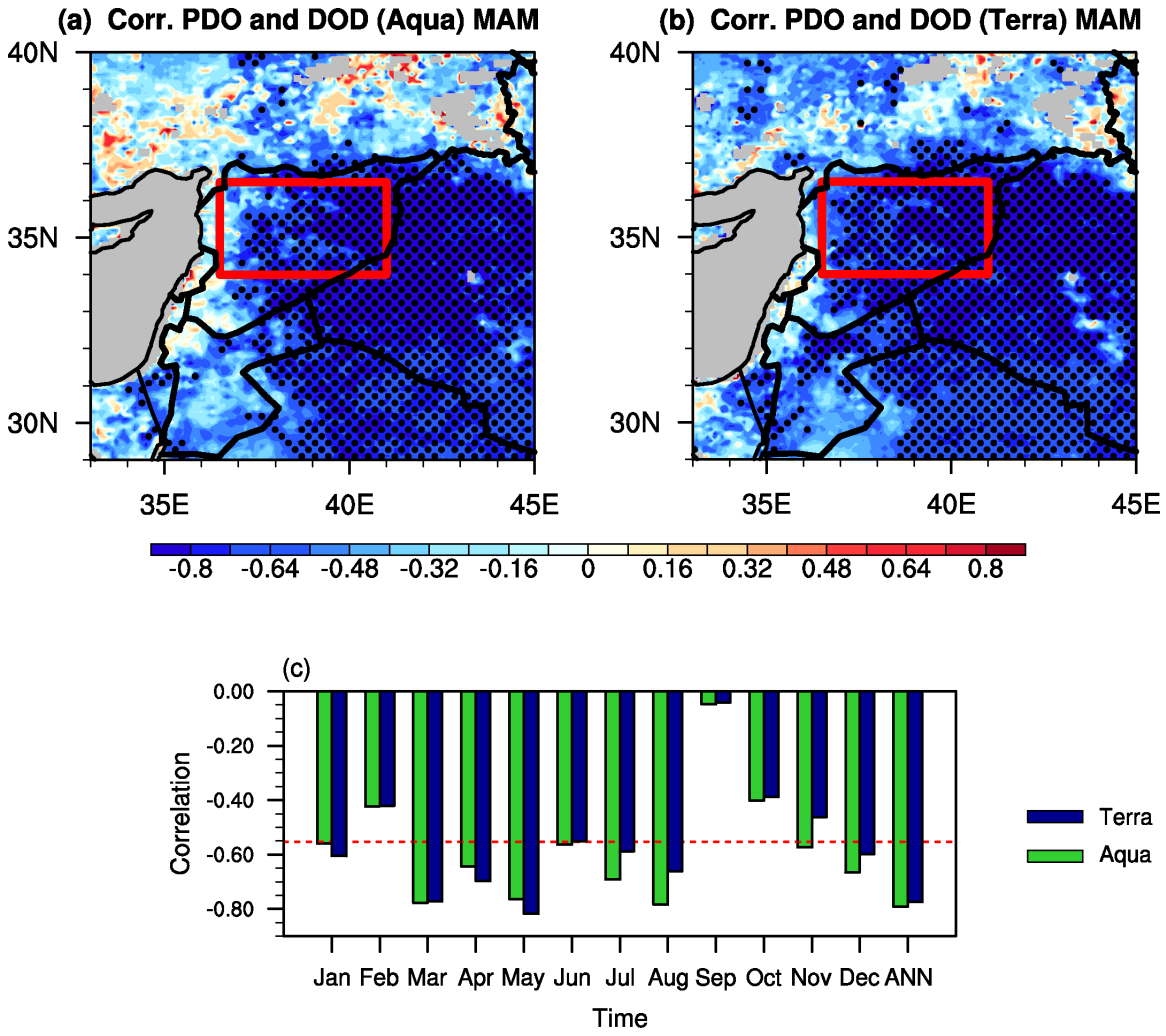

Figure 2. Correlation between the PDO index and MODIS (a) Aqua and (b) Terra DOD in MAM from 2003-2015. (c) Correlation between Syrian DOD indices (navy and green bar denotes Terra and Aqua, respectively) and PDO index for each month and annual mean (ANN) from 2003 to 2015. Red dashed lines denote the 95% confidence level (t test). Red box denotes the averaging area for Syrian DOD index.

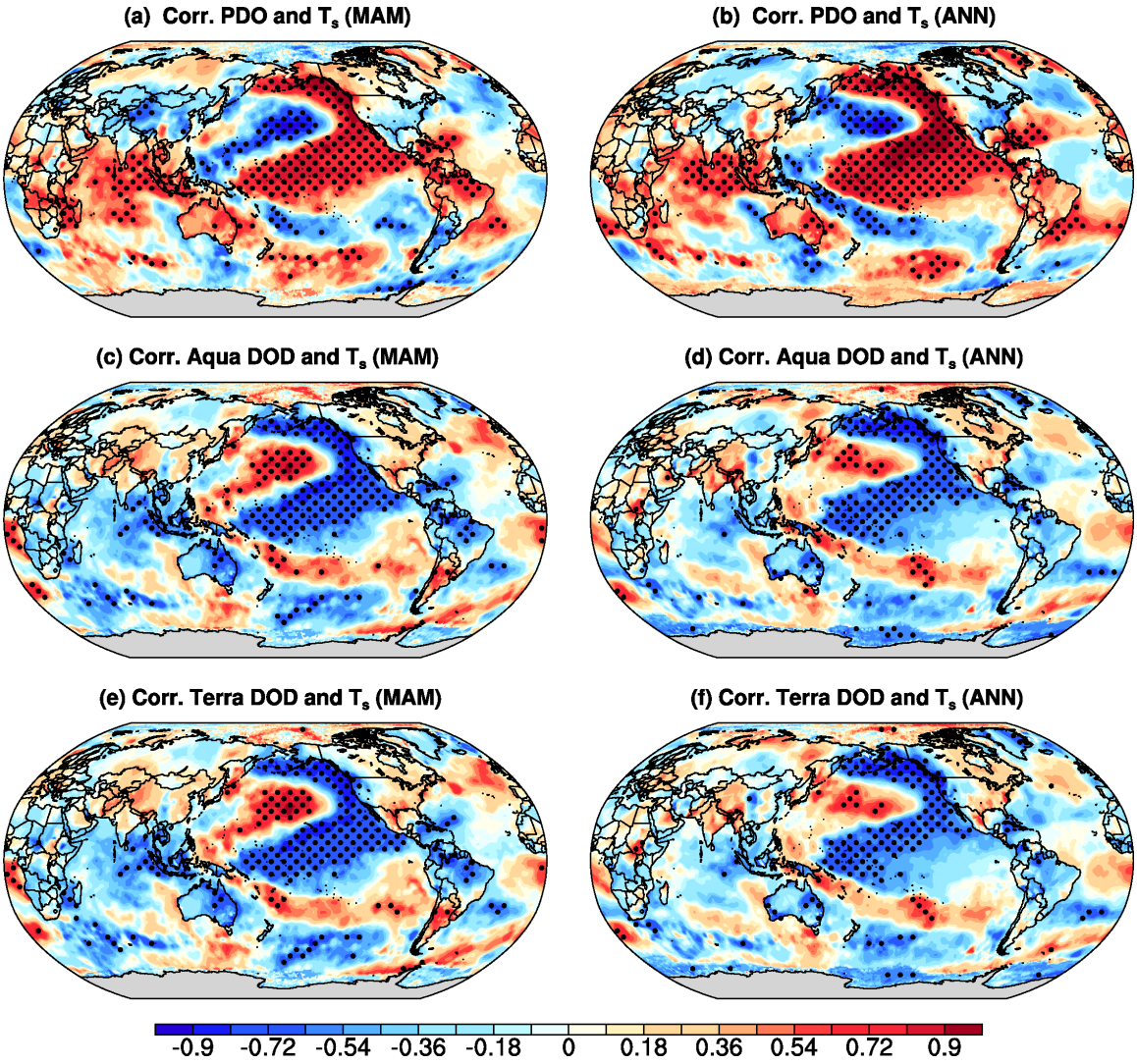

Figure 3. Correlation between the PDO index and HadISST (over the ocean) and CRU TS3.23 near-surface temperature (over land) for (a) MAM and (b) annual mean during 2003-2014. Correlation between (c)-(d) Aqua and (e)-(f) Terra DOD indices and HadISST and CRU near-surface temperature for (c), (e) MAM and (d), (f) annual mean during 2003-2014. Areas significant at the 95% confidence level (t-test) are dotted.

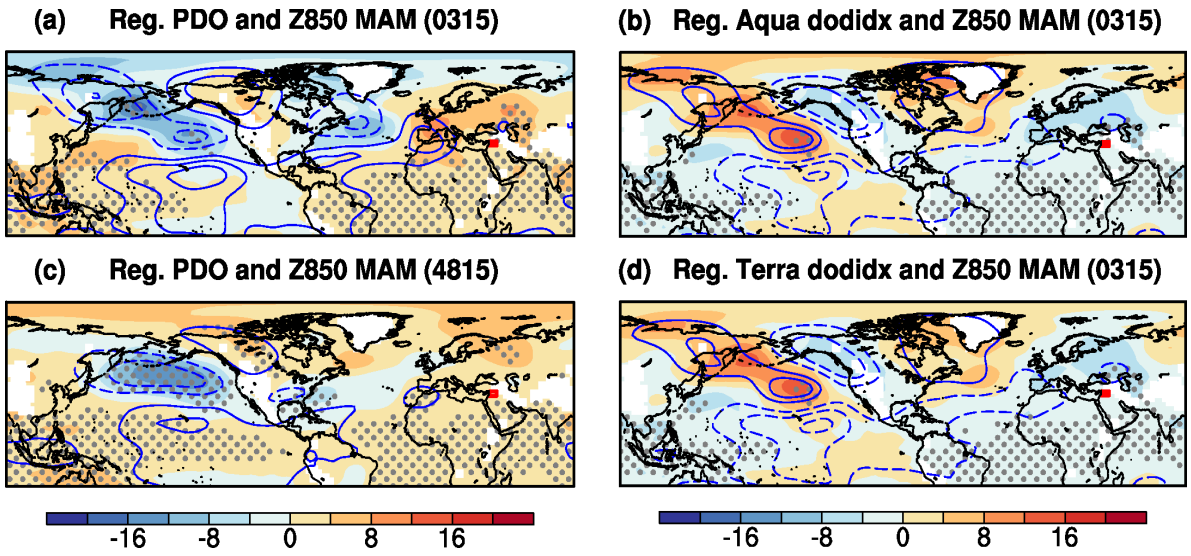

Figure 4. Regression of 850 hPa (shading) and 200 hPa (blue contours; solid lines for positive values and dashed lines for negative values, from -40 gpm to 40 gpm with an interval of 10 gpm, zero line is not shown) geopotential heights onto the standardized PDO index for (a) 2003-2015 and (c) 1948-2015 and onto the standardized (b) Aqua and (d) Terra DOD indices. Areas significant at the 95% confidence level (t-test) are dotted.

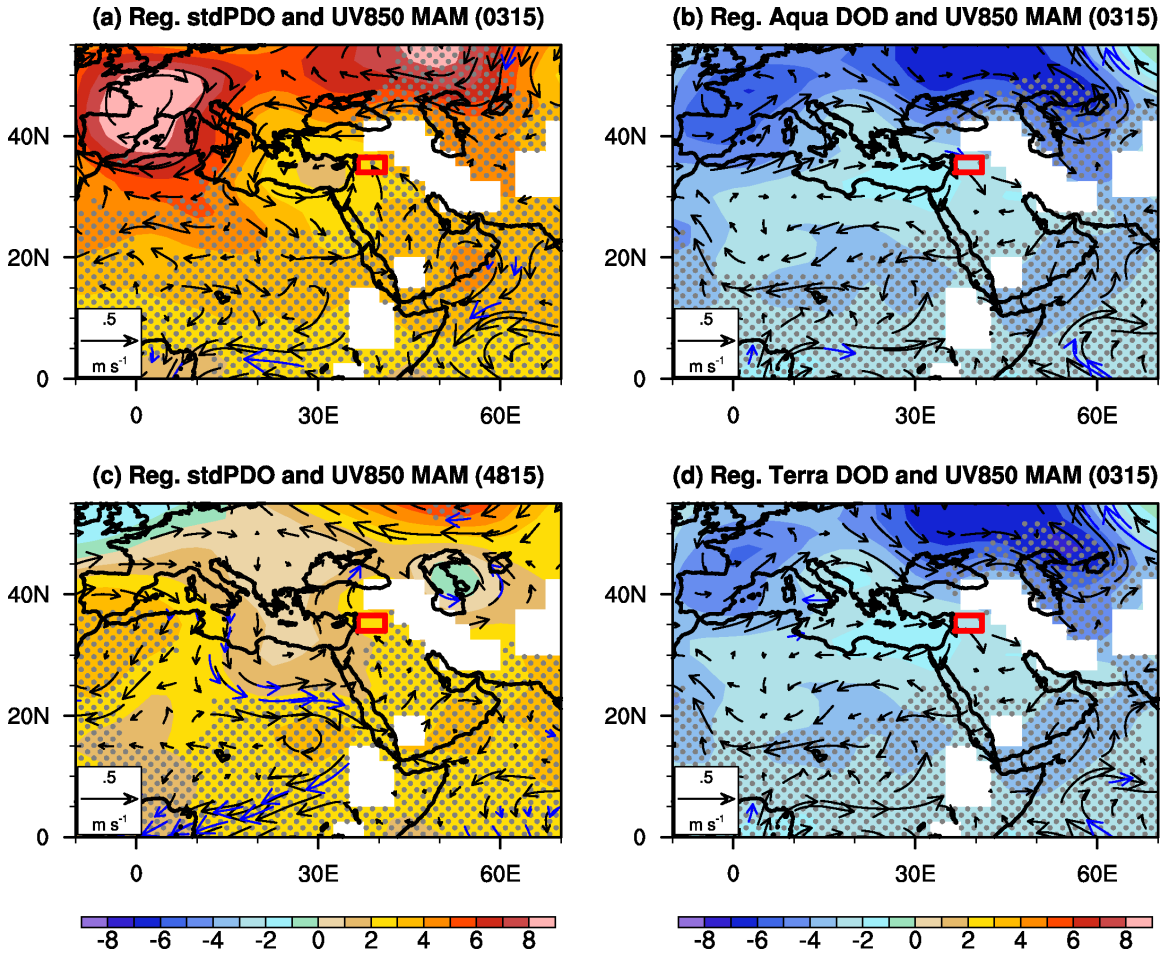

Figure 5. Regressions of NCEP1 850 hPa geopotential height (shading; gpm) and horizontal winds (vectors; m s^{-1}) onto the standardized PDO index during (a) 2003-2015 and (c) 1948-2015, and onto the standardized (b) Aqua and (d) Terra DOD indices during 2003-2015. Area where the regression is significant at the 95% confidence level (t-test) is dotted, and vectors significant at the 90% confidence level are plotted in blue.

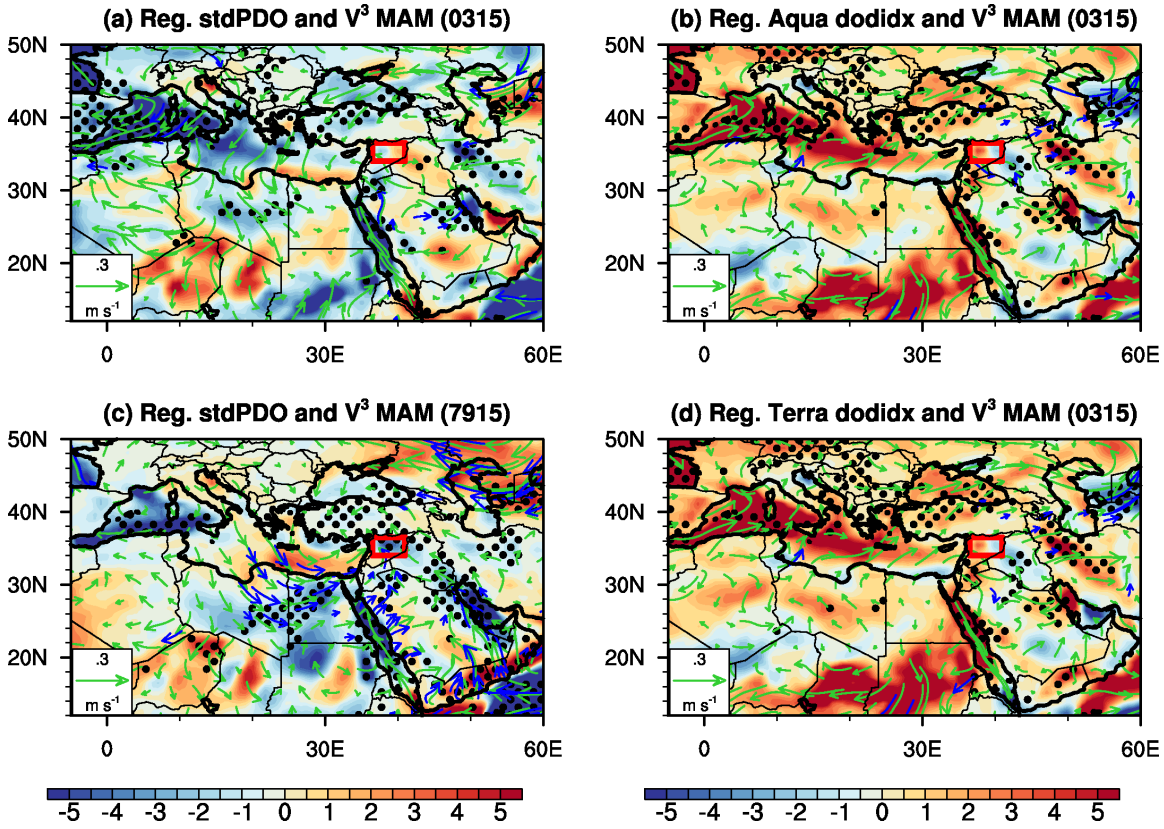

Figure 6. Regressions of ERA-Interim 10 meter horizontal winds (green vectors; m s^{-1}) and cubic wind speed (shading; m^3 s^{-3}) onto standardized PDO index (a) from 2003-2015 and (c) from 1979-2015 and onto the standardized (b) Aqua and (d) Terra DOD indices. Areas where the regressions of the wind speed are significant at the 95% confidence level are dotted and vectors significant at the 90% confidence level are plotted in blue (t-test).

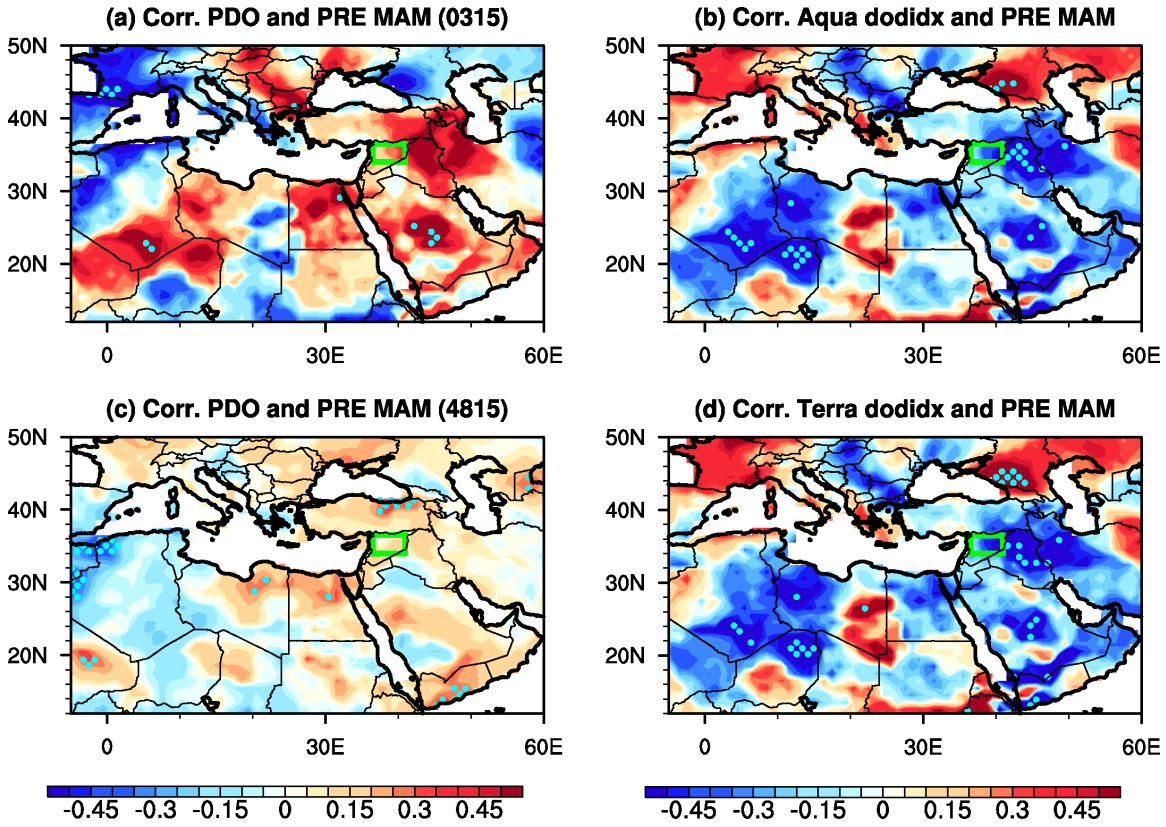

Figure 7. Correlation between PRECL precipitation and PDO index during (a) 2003-2015, (c) 1948-2015 and between precipitation and (b) Aqua and (d) Terra DOD indices during 2003-2015. Areas where the correlation coefficients are significant at the 95% confidence level (t-test) are dotted.

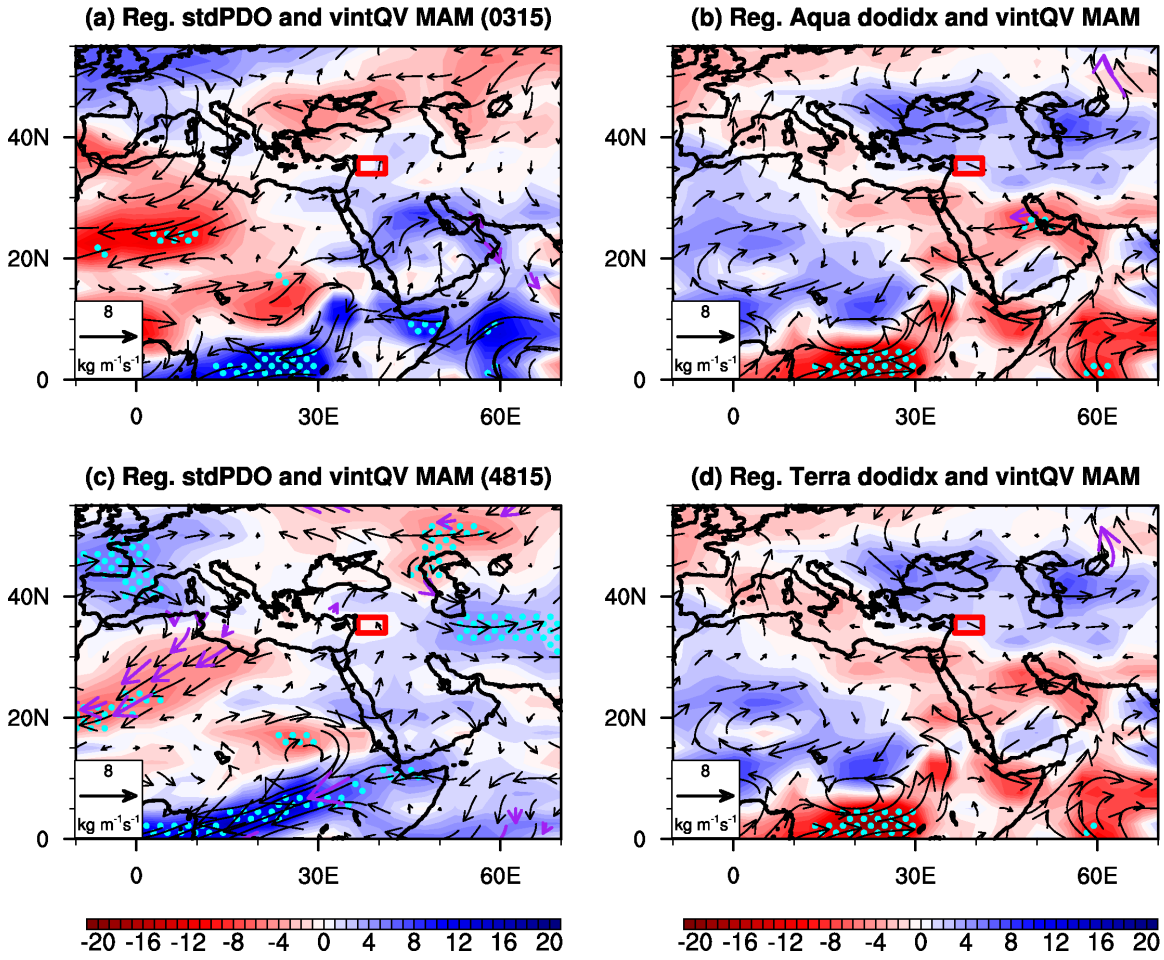

Figure 8. Regression of vertically integrated mass weighted monthly moisture flux (vectors; kg m^{-1} s^{-1}) and its magnitude (shading) onto standardized PDO index during (a) 2003-2015 and (c) 1948-2015, and onto the standardized (b) Aqua and (d) Terra DOD indices. Moisture flux is integrated from surface to 300 hPa. Areas with magnitude of moisture flux significant at the 90% confidence level are dotted, and moisture fluxes significant at the 90% confidence level are plotted in purple vectors (t-test).

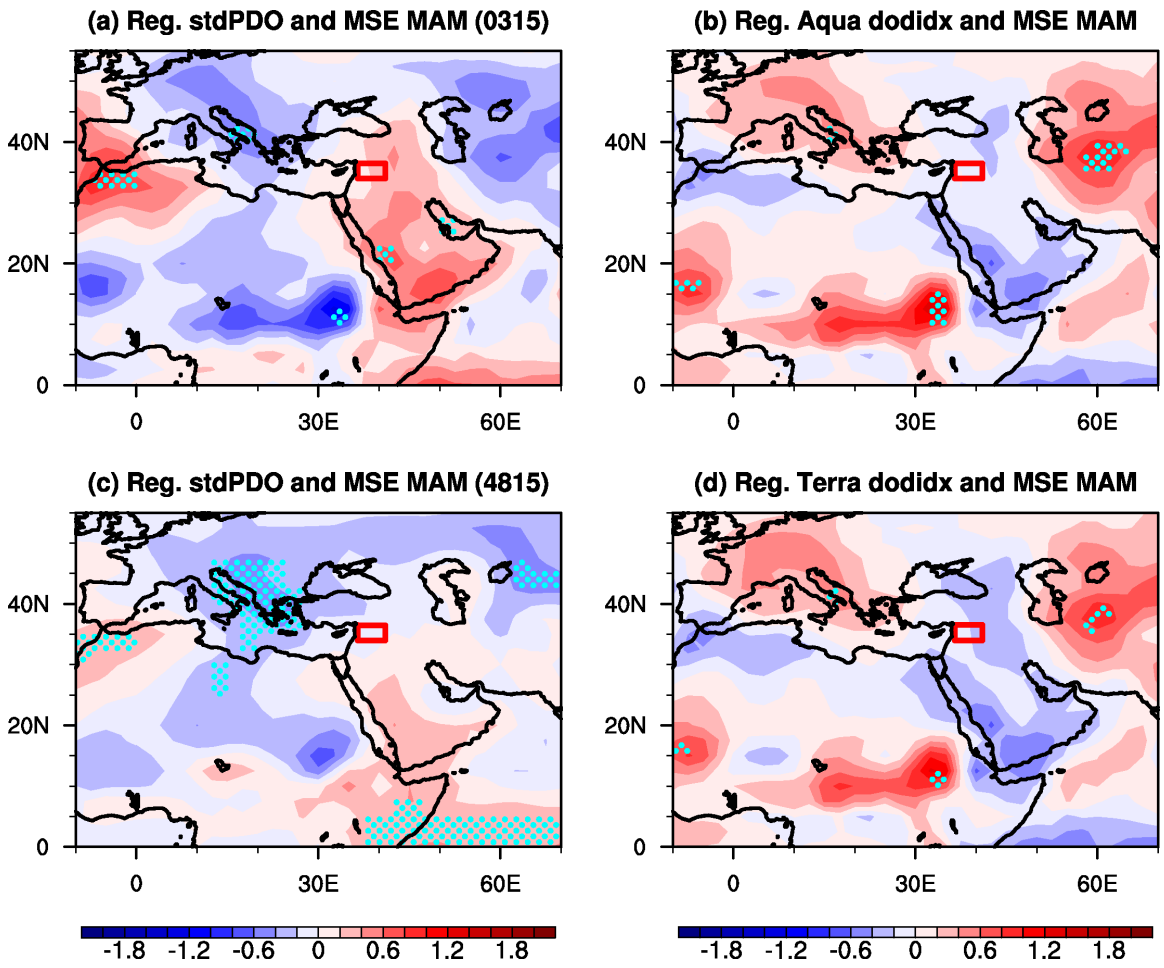

Figure 9. Regression of vertically integrated MSE (10^4 J m^{-2}) over the lowest four atmospheric layers (1000, 925, 850, and 700 hPa) from the NCEP1 onto the standardized PDO index for (a) 2003-2015 and (c) 1948-2015 and onto the standardized DOD indices from MODIS (b) Aqua and (d) Terra during 2003-2015. Areas significant at the 90% confidence level (t-test) are dotted.

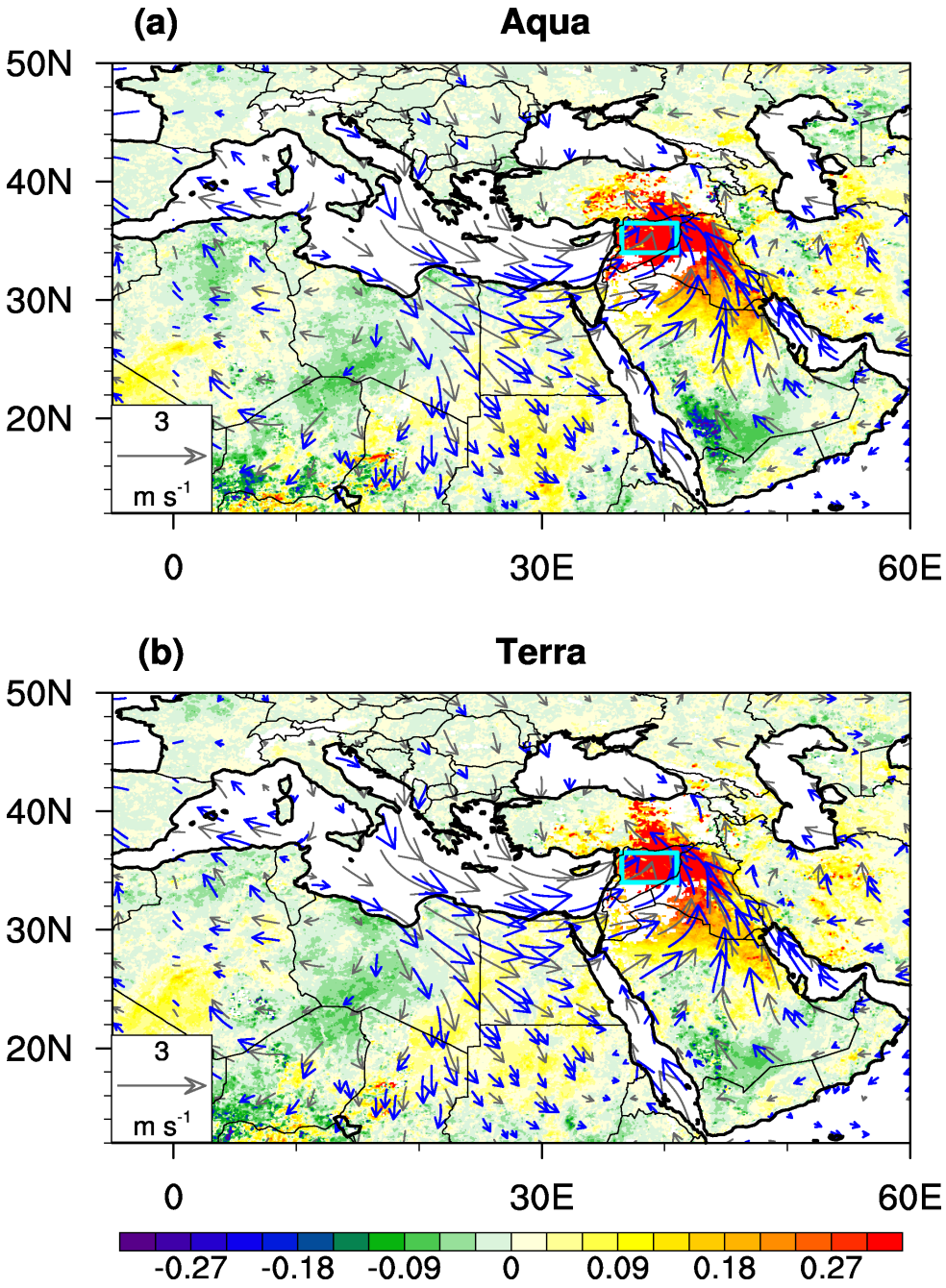

Figure 10. Composites of (a) Aqua and (b) Terra daily DOD (shading) along with ERA-Interim 10 m horizontal wind anomalies (with reference to the 1979-2015 mean; vectors) for days with Syrian DOD index (Aqua) greater than 1 standard deviation during MAM from 2003-2015. Shading shows values significant at the 95% confidence level over land, while wind vectors significant at the 95% confidence are plotted in blue (t-test).

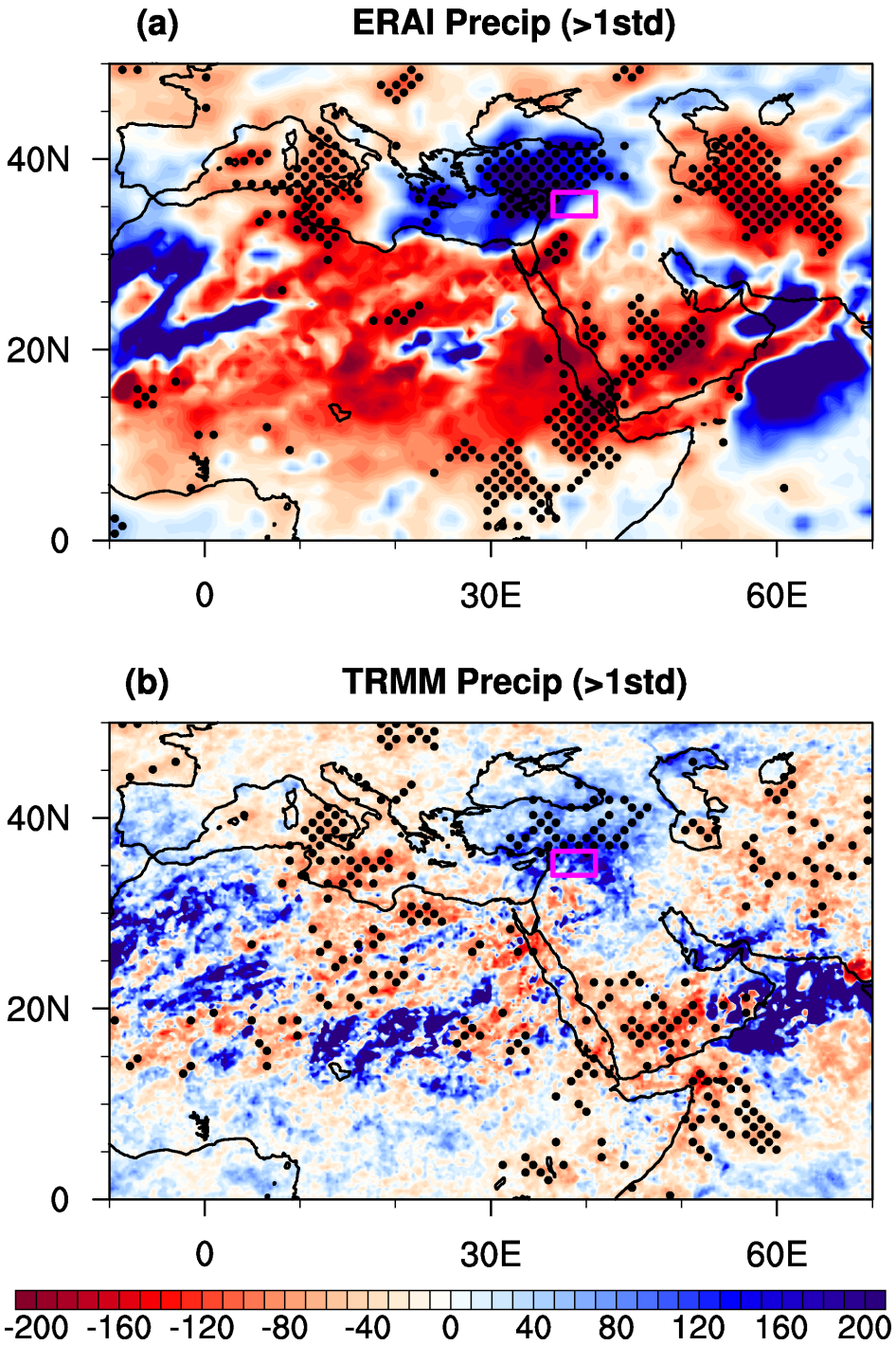

Figure 11. Composites of daily precipitation anomalies (shading; % with references to the climatology) from (a) the ERA-interim and (b) TRMM for the days with Syrian DOD index (Aqua) greater than 1 standard deviation during MAM from 2003-2015. Areas significant at the 95% confidence level (t-test) are dotted.

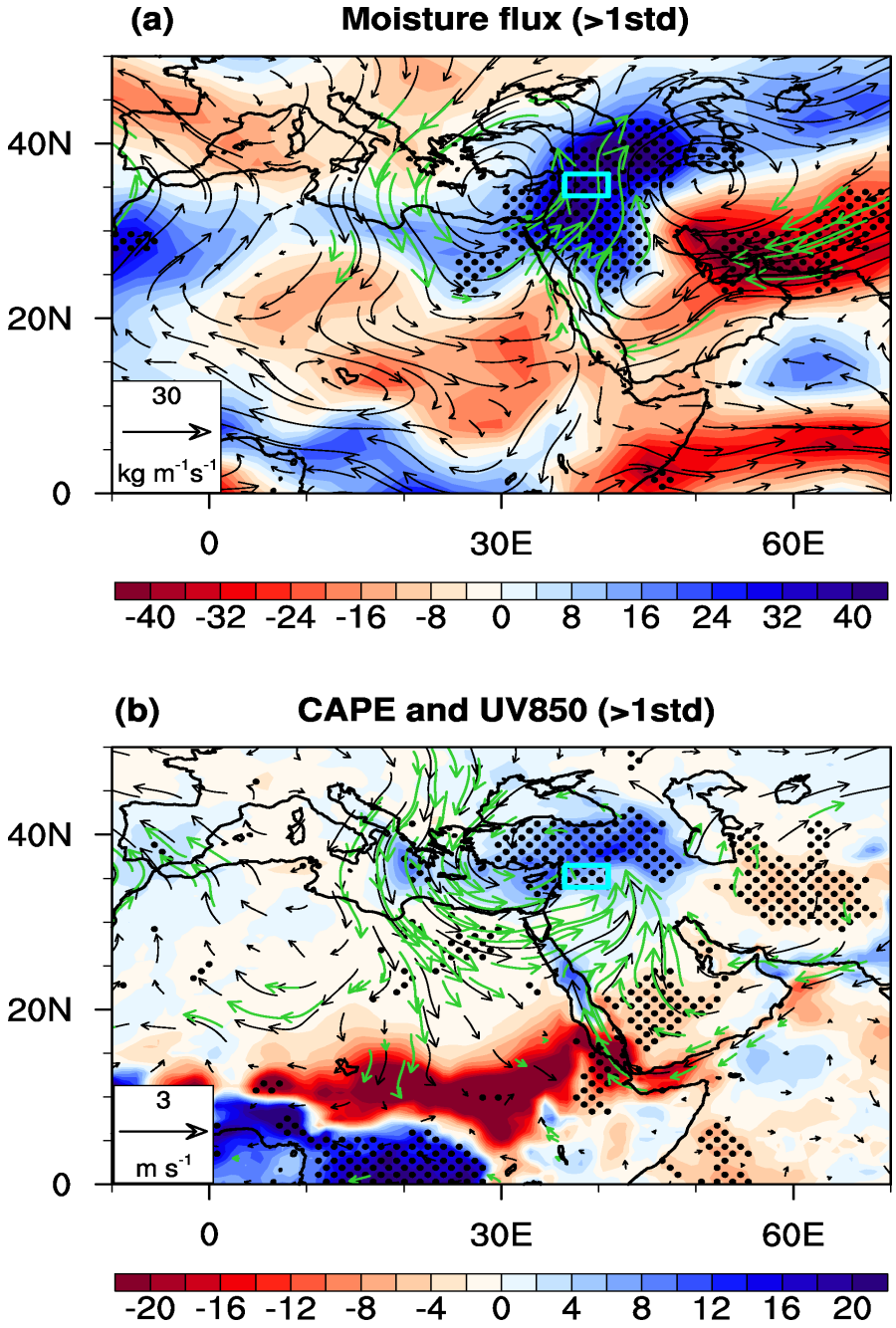

Figure 12. Composites of (a) vertically integrated mass-weighted moisture flux (vectors; kg $m^{-1}s^{-1}$) and its magnitude (shading) from the NCEP1 and (b) CAPE (10^4 J/kg) along with 850 hPa winds (m s^{-1}) from the ERA-Interim for the days with Syrian DOD index (Aqua) greater than 1 standard deviation during MAM from 2003-2015. Moisture flux is integrated from surface to 300 hPa. Shading areas significant at the 95% confidence level are dotted.

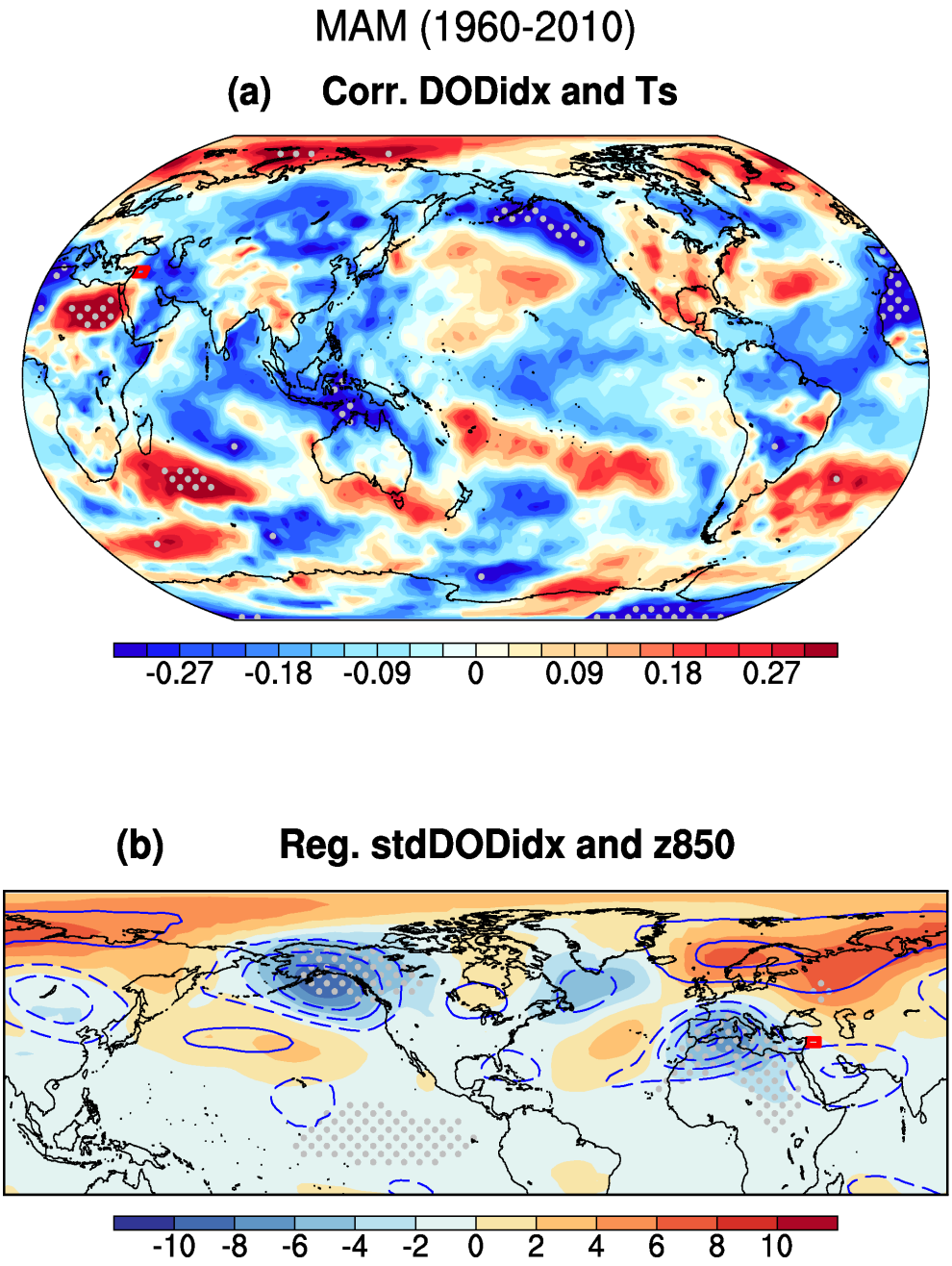

Figure 13. (a) Correlation between AM3 DOD index averaged over Syria (see Fig. 2) and surface temperature from 1960-2010 and (b) regression of 850 hPa (shading) and 200 hPa (contours; solid lines for positive values and dashed lines for negative values, from -20 gpm to 20 gpm with intervals of 5 gpm, zero line is not shown) geopotential height onto the standardized DOD index from 1960-2010. Shading areas significant at the 95% confidence level are dotted.